UNIVERSIDADE FEDERAL DE PERNAMBUCO
CENTRO DE TECNOLOGIA E GEOCIÊNCIAS
DEPARTAMENTO DE ENGENHARIA CIVIL E AMBIENTAL
PROGRAMA DE PÓS-GRADUAÇÃO EM ENGENHARIA CIVIL

RAYRA AMORIM SILVA

PRINCIPAL COMPONENT ANALYSIS FOR THE PROCESS OF OPENING UNDERGROUND CAVERNS IN SALT ROCKS

Recife
2022

RAYRA AMORIM SILVA

PRINCIPAL COMPONENT ANALYSIS FOR THE PROCESS OF OPENING UNDERGROUND CAVERNS IN SALT ROCKS

Dissertation presented to the Post-Graduate Program in Civil Engineering at the Federal University of Pernambuco as a partial requirement for obtaining a Master's degree in Civil Engineering.

Concentration area: Oil Reservoir Simulation and Management.

Advisor: Prof. Dr. Leonardo José do Nascimento Guimarães.

Recife

2022

Catalogação na fonte:
Bibliotecária Sandra Maria Neri Santiago, CRB-4 / 1267

S586p Silva, Rayra Amorim.
Principal component analysis for the process of opening underground caverns in salt rocks / Rayra Amorim Silva. – 2022.
91 f.: il., figs., tabs., abrev. e siglas.

Orientador: Prof. Dr. Leonardo José do Nascimento Guimarães.
Dissertação (Mestrado) – Universidade Federal de Pernambuco. CTG. Programa de Pós-Graduação em Engenharia Civil. Recife, 2022.
Inclui referências e apêndice.

1. Engenharia civil. 2. Caverna. 3. Rocha salina. 4. Variáveis de processo. 5. Simulações numéricas. 6. Análise estatística. I. Guimarães, Leonardo José do Nascimento (Orientador). II. Título.

UFPE

624 CDD (22. ed.) BCTG/2022-306

RAYRA AMORIM SILVA

PRINCIPAL COMPONENT ANALYSIS FOR THE PROCESS OF OPENING UNDERGROUND CAVERNS IN SALT ROCKS

Dissertation presented to the Post-Graduate Program in Civil Engineering at the Federal University of Pernambuco, Center of Technologic and Geosciences as a partial requirement for obtaining a Master's degree in Civil Engineering. Concentration Area: Oil Reservoir Simulation and Management

Aprovada em: 28/03/2022.

Orientador: Prof. Dr. Leonardo José do Nascimento Guimarães - UFPE

BANCA EXAMINADORA

_____
Prof. Dr. Igor Fernandes Gomes (Examinador Interno)
Universidade Federal de Pernambuco

_____
Prof. Dr. Bernardo Horowitz (Examinador Interno)
Universidade Federal de Pernambuco

_____
Prof. Dr. Edgard Poiate Junior (Examinador Externo)
Petrobras

I dedicate this work to my family, especially my mother and sister, you were the strength and fuel for the most difficult days!

ACKNOWLEDGEMENTS

Words are not enough to express the gratitude for completing another step. Over these three years, there were many challenges, moments when I thought about giving up, a world in chaos, but the will to win and overcome were greater and here I am, showing that it was possible.

I thank God first, because everything happens according to his providence and to him I am grateful for everything that I am and that I have.

To my parents, Luís and Francisca and my brothers, Mayra and Luan, without you none of this would be possible, my greatest asset, thank you for your unconditional support as always.

To my advisor, Leonardo, for all the teachings passed on and for believing in my ability, you certainly were an example of a master and dedication in what you do.

To the other professors in my area of concentration, my sincere thanks for their patience and for sharing their experiences with us.

To LMCG colleagues, gratitude for all the conversations, exchanges and “ear pulling”.

To my colleagues from “Caverna”, thank you for your receptivity, patience and for all your help, I am very grateful for everything I learned in this project.

To the administrative team, Rose, Priscila, Andrea, Cleide and Juliana, for all the support and good times.

À CAPES, Petrobras and Energi Simulation for their financial support.

To my family members who, even from afar, were present in thoughts and cheers.

To my master's friends and housemates, Renata and Joelma, thank you for all the care, affection and shared experiences.

To the other master's friends, Geovana, Layane, Ádria, Alexandre, I am grateful for all the help and knowledge shared.

To the friends that Recife and crossfit gave me, Carolzinha, Carol and Cath, for all the experiences and unique moments.

Finally, thank you all very much!

"This study was financed in part by the Coordenação de Aperfeiçoamento de Pessoal de Nível Superior - Brasil (CAPES) - Finance Code 001".

ABSTRACT

The constant dynamism within the oil industry associated with the need for new technologies in terms of production and disposal of products were fundamental for the increase of studies about the use of underground caverns in salt rocks as an alternative for the storage of petroleum products. Salt rock is particularly useful for storage because of its low cost, low permeability, and its healing potential when compared to other rocks, including granite, mud, and basalt. The opening process and subsequent development of these cavities are complex activities and the variables involved in the process play a crucial role during the entire operation. In this sense, the present work aims to identify, through the PCA (Principal Component Analysis) statistical tool, the variables that most influence the process of opening a salt cavern by dissolution. For this, numerical simulations of the dissolution mining process for opening a cavern under typical conditions of water injection into a salt rock using the software SALGAS were developed considering different methods of saline water circulation, after that, the variables injection temperature, injection rate, radius, volume, pump power, cumulative energy, tubing loss, produced brine, pump pressure, injection pressure, and salt dissolution factor were interpreted using the multivariate statistical tool through software PAST. For the simulations generated, the results with the statistical tool were satisfactory, it was found that the brine injection rate contributes significantly to the process, in terms of x-axis, directly influencing the behavior of other variables, the temperature have a great importance to the y-axis. Regarding the total variability of the data, more than 97% of these could be represented in terms of the first two components for both scenarios studied.

Keywords: cavern; salt rock; process variables; numerical simulations; statistical analysis.

RESUMO

O constante dinamismo dentro da indústria do petróleo associado a necessidade de novas tecnologias em termos de produção e escoamento de produtos foram peças fundamentais para o aumento de estudos sobre a utilização de cavernas subterrâneas em rochas salinas como alternativa para o armazenamento produtos petrolíferos. A rocha salina é particularmente útil para o armazenamento devido ao seu baixo custo, baixa permeabilidade e seu potencial de cicatrização. O processo de abertura e posterior desenvolvimento dessas cavidades são atividades complexas e as variáveis envolvidas no processo desempenham papel fundamental durante toda a operação. Neste sentido, o presente trabalho tem por objetivo identificar através da ferramenta estatística PCA (*Principal Component Analysis*), as variáveis que mais influenciam no processo de abertura da caverna por dissolução. Para isso, simulações numéricas do processo de mineração por dissolução para abertura de uma caverna sob condições típicas de injeção de água em uma rocha de cloreto de sódio utilizando o *software* SALGAS foram desenvolvidas considerando métodos diferentes de circulação da água salina. Após isso, as variáveis temperatura de injeção, taxa de injeção, raio, volume, potência da bomba, energia acumulada, perda de carga na tubulação, salmoura produzida, pressão da bomba, pressão de injeção e fator de dissolução do sal foram interpretadas usando a ferramenta estatística multivariada através do *software* PAST. Para as simulações geradas, os resultados com a ferramenta estatística foram satisfatórios, constatou-se que a taxa de injeção da salmoura contribui significativamente para o processo, em termos do eixo x, influenciando diretamente no comportamento de outras variáveis, a temperatura teve uma grande importância para o eixo y. Em relação a variabilidade total dos dados, mais de 97% destes puderam ser representados em termos das duas primeiras componentes para ambos os cenários estudados.

Palavras-chave: caverna; rocha salina; variáveis de processo; simulações numéricas; análise estatística.

LIST OF FIGURES

LIST OF TABLES

LIST OF ABBREVIATIONS AND ACRONYMS

AD	Anno Domini
BC	Before Christ
D	Direct
DOE	Department of Energy
FDM	Finite Difference Method
FORTRAN	Formula Translator
ID	Injection Depth
PAST	Paleontological Statistics
PC	Principal Component
PCA	Principal Component Analysis
PD	Production Depth
R	Reverse
RSDUGI	Rock Salt Dissolution at Underground Gas Industry
SALGAS	Solution Mining Simulation Software
SMRI	Solution Mining Research Institute
SPR	Strategic Petroleum Reserve
TWH	Two-Well-Horizontal
TWHSMC	Two-Well-Horizontal Solution Mining Cavern
TWV	Two-Well-Vertical
3D	Three Dimensional
UHS	Underground Hydrogen Storage
UGS	Underground Gas Storage

LIST OF SYMBOLS

ρ_b	Density of the saline solution to be injected
c_b	Mass salt concentration
v	Specific volume of injection fluid
A, ..., H	Injection fluid temperature functions
$\varphi_{0,1,2,11,12}$	Coefficients for calculating functions A,B,C,D,E,F,G and H
ρ_w	Pure water density
a_i e b_i	Constants
P^{ref}	Reference pressure
c_b^{sat}	Mass salt concentration present in saturated brine
m_T	Rate of dissolution of a brine
ρ	Specific density of a brine
T_0	Reference temperature
T	Initial production temperature
DF	Dissolution factor
P	Injection pressure
P_1	Fluid pressure to be injected
P_2	Fluid pressure in the massive
g	Gravity acceleration
v	Velocity
z	Height
γ	Specific weight
P_i	Pressure at the height of each valve
H_i	Injection valve height
$X_{1, ..., p}$	Dependent original variables
n	Number of observations
π	Population
p	Number of characteristics
X	Original data matrix
$\underline{\boldsymbol{X}}$	Data average
z_{ij}	Standardized values
x_i	Samples for i = 1,2, ..., n e j = 1,2, ..., p

$\underline{\boldsymbol{x_j}}.$	Estimative of the average of characteristic j
$s(x_j)$	Standard deviation of characteristic j
'S'	Covariance matrix
'R'	Correlation matrix
$Y_{1, ..., p}$	Independent variables
Z	Standardized matrix
I	Identity matrix
λ_i	Eigenvalues
$\widetilde{e_i}$	Eigenvectors
var(Yi)	Variance of the transformed variables
$cov(Y_iY_j)$	Covariance of independent variables
C_i	Contribution of each principal component
Trace (S)	Trace of matrix S
k	New data dimension
$\boldsymbol{Corr(X_jY_i)}$	Correlation between each X_j and the Y_i component
w_i	Weight of each variable on the component

SUMMARY

1 INTRODUCTION

The growing global energy demand serves as a lever for the search for new techniques for the safe storage of petroleum products and waste in general. In this sense, rock salt is considered the ideal material for underground storage due to its low permeability, healing capacity and availability (NAZARY MOGHADAM et al., 2015). Other modals such as saline aquifers and depleted oil and gas formations have as limitations are subjected to regional pressure build-up because of water movement, which might affect reservoir integrity, in case of aquifers (HAMZA et al., 2021) and the lower capacity of depleted reservoirs when compared to others modals.

In addition, underground salt caverns can be built by dissolution mining techniques, which are cheaper than other conventional excavation techniques (NAZARY MOGHADAM et al., 2013). When compared to other rocks, including granite, mud and basalt the cost of leaching caverns by dissolution using the salt rock turns out to be lower. Another advantage is the ability to absorb harmful nuclear radiation (in a waste storage medium and water solubility, an ideal choice for deep burial of nuclear waste and oil and gas storage) (YANG et al., 2017).

The dissolution of the salt rock contemplates the initial phase of opening of these cavities, being one of the first experimental studies on the subject, that of DURIE & JESSEN (1964) who carried out a series of laboratory tests in order to evaluate the influence of the injection rate of water (fresh and salt) in the cavern formation rate and in the salt removal rate. In addition to experimental studies, mathematical and numerical modeling were also developed. Also, in the work of DURIE & JESSEN (1964) a mathematical model was presented that describes the dissolution process as a function of the salinity of water at any point on the vertical surface of the salt. It was found that at low injection rates, the induced flow does not significantly contribute to the salt removal rate.

SABERIAN (1974) developed a 5” tall cylindrical model to study the flow and expansion mechanisms of salt cavities during dissolution, the results combined into a generalized numerical model, where the prediction of cavity dissolution as a function of the time and also other physical parameters such as speed, radius and dissolution rate. More recently YANG et al. (2017) presented a proposal for an analytical solution of a differential equation to calculate the dissolution rate of salt rocks subjected to an

instantaneous diffusion process, the results showed a fit between the numerical model and the experiment of the salt concentration with respect to time.

As these are numerical aspects, the parameters involved in numerical simulations can also be interpreted from a statistical perspective. Multivariate data analysis can reduce data or carry out a structural simplification as well as investigate the dependency relationship between variables (FERREIRA, 2011). This set of statistical methods is widely used in various fields of science and encompasses different techniques, the most used being cluster analysis, factor analysis, principal component analysis, multiple regression and logistic regression, each with its own characteristics. In the present work, the variables are studied using the Principal Component Analysis (PCA) technique. In this method, an orthogonal transformation is performed to convert a set of observations of possibly correlated variables into a set of values of linearly uncorrelated variables called Principal Components (PC) that reveal the internal structure of the data in a way that best explains its variance (ALONSO-GUTIERREZ et al., 2015).

The objective of this technique is to find a new set of variables with lower dimensionality than the original set, so that it is possible to preserve most of the information contained in the data. In addition to explaining the total variation, this analysis also allows us to investigate the dependency relationship between the variables and the degree of influence each one has individually for the object of study of the research.

1.1 MOTIVATION

The production and development plants within the oil industry rely on fast processes, massive structures that demand space and money, especially in an offshore environment where the flow of production and also the safe disposal are somewhat compromised due to the distance in relation to safe collection or storage locations, depending in most situations on long and expensive transmission lines. Given this situation, the opening and subsequent operation of underground salt caverns using the dissolution mining technique has gained an attractive space as a solution for the safe storage of petroleum products and waste in general.

In addition to the economic factor that highlights the dissolution mining technique from other conventional salt cavern leaching techniques, field studies

using this technique also produced good results, reaffirming its great operability. One of them was developed by FAIRCHILD et al. (1999) who completed a field test study of the dissolution characteristics of NaCl, and found a positive correlation between dissolution rate and exposure surface area. More recently, LIU et al. (2016), based on rock salt dissolution test data, established a dynamic rock salt dissolution model under gravity, which is solved using the finite difference method, which can provide basic parameters of cavern construction of rock salt.

These and other experimental tests served as a basis to understand the behavior of these caverns with the dissolution of the salt. Complementing this, it is also necessary to know the best dissolution strategy, the variables that exert greater influence on the process and the final behavior of the cavities. The final performance analysis can be achieved through the generation of response surfaces, obtained for example through finite difference and finite element programs that are able to predict the behavior of these salt cavities, a situation that was only possible before analyzed based on experience with other caverns nearby. In the present work the Finite Difference Method (FDM) is used to predict response surfaces for these caverns, this method solves differential equations based on the finite difference derivative approximation. The main motivation for using such a numerical tool lies in the fact that it is widely used, highly efficient and capable of producing satisfactory simulations for the studied scenarios.

After the surface generation, the numerical data analysis was performed with the PCA statistical tool. As the underground cavern opening process in salt rock involves a variety of parameters, this method will allow to investigate the degree of individual contribution that each of these variables provide to the process. This study allows other studies that are more focused on the most effective variables to be developed, in addition to being a point of improvement for those that contributed to a lesser degree.

1.2 OBJECTIVE

In this section, the objectives of this dissertation will be presented.

1.2.1 General Objective

This dissertation has as general objective to use the technique of multivariate statistical analysis PCA (Principal Component Analysis) to identify the variables that most influence in the process of opening an underground cavern in saline rock. The numerical data used by this method are produced from numerical simulations of the opening of this same cavern by dissolution, using the finite difference software SALGAS.

1.2.2 Specific Objectives

- ❖ Evaluate cavern geometry over time;
- ❖ Identify, regarding the type of mining, the most favorable scenario for the opening of this salt cavern by dissolution;
- ❖ Reduce the dimensionality of numeric data, preserving most of the information contained in the data.
- ❖ Analyze the dependency relationship between the variables;
- ❖ Explain the variability of data generated with numerical simulations;
- ❖ Quantify the influence of the variables brine production rate and temperature of the injected water in the process of opening the salt cavern by dissolution.

1.3 ORGANIZATION OF THE DISSERTATION

The present work is organized into eight chapters, whose content is briefly described below.

- **Chapter 1 – Introduction:** presents the context, the motivation of the topic discussed and the objectives you want to achieve.
- **Chapter 2 – Salt Caverns:** theoretical aspects and methodologies for the construction of salt caverns using the dissolution mining technique are discussed. In addition, some mathematical models, numerical and experimental tests used to study the opening of these caves are also discussed.
- **Chapter 3 – Caverns Opening with the SALGAS:** defines, characterizes and highlights the main advantages and limitations of the SALGAS software, in addition to presenting the equations that govern the calculation of input data for the program.
- **Chapter 4 – PCA and the Use of the PAST Software:** defines, characterizes, highlights the main advantages and limitations and presents the mathematical development of the PCA statistical tool, in addition to the use of the PAST software.
- **Chapter 5 – Methodology**: the solution mining scenarios for the opening of the underground cavern in salt rock are discussed with the description of the input data for the SALGAS software and for the PAST software.
- **Chapter 6 – Results and Discussions:** presents the main simulations obtained with the SALGAS software and the statistical analysis with the PAST software.
- **Chapter 7 – Conclusions:** describes the conclusions obtained according to the pre-established objectives.
- **Chapter 8 – Suggestions for Future Work.**

2 SALT CAVERNS

In this chapter, the theoretical aspects and methodologies of the construction of salt caverns using the dissolution mining technique are discussed. In addition, some mathematical models, numerical and experimental tests used to study the opening of these caverns are also discussed.

The salt rocks solution mining is currently one of the most widely used leaching methods, although there is no broader scientific database on the subject in the literature, it is known that the predominant factor for its choice is the low cost economic combined with the excellent properties of salt rock. Its first use records date back to approximately 250 BC in China, where wells were drilled in deep salt deposits, for injection and production of the brine, bamboo tubes were used, the basis of current technology had its origins in France, around 858 AD (DE MELO et al., 2008). It is believed that possibly the first record of the production-scale solution mining method is associated with the Spanish in 1752 (JEREMIC, 1994).

The history of the solution mining technique sometimes remains closely related to the history of salt caverns, since the first is a typical technique for generating the second and many studies have been developed in order to find efficient ways to dissolve these cavities, among these, the work produced by DURIE & JESSEN (1964) was one of the most explored. Efficient dissolution contributes to the good development of the cavern and, consequently, satisfactory response surfaces are generated.

The first underground salt cave design used for liquids and gases was reported in Canada in the early 1940s, later salt cave storage quickly spread to the US and European countries (YIN et al., 2020).

In the USA, the fear of maintaining greater dependence on foreign oil sources was decisive for the American Congress to approve, in December 1975, the Law on Energy Policy and Conservation. This act gave the requirements of a Strategic Petroleum Reserve (SPR) of up to one billion barrels of crude oil, The United States Department of Energy (DOE) was in charge of the overall responsibility of the SPR. After careful consideration, the decision was made to store the reserve in conventionally mined caverns in underground salt dome formations along the Gulf Coast (QUERIO et al., 1981). The region comprises two locations in the state of

Texas (Bryan Mound and Big Hill) and two in the state of Louisiana (West Hackberry and Bayou Choctaw). Built deep in the massive salt deposits that support most of the Texas and Louisiana coast, the caves offer the best security and are the most affordable storage media, costing up to 10 times less than above-ground tanks and 20 times less than hard rock mines, these four sites currently have a combined authorized storage capacity of 714 million barrels (U.S. DEPARTMENT OF ENERGY, 2020).

Unlike in the USA, the study of salt caverns in China started late, knowing about the successful experiences with saline caves in other countries, Chinese researchers studied the behavior of this rock, among them YANG et al. (1999) who carried out an experimental study of the creep behavior of salt, attesting to its capacity to function as a host rock for the storage of hydrocarbons. Quite unlike the largely thick salt domes, salt formations in China are highly heterogeneous with thin layers, characterized by the presence of numerous halite layers, high impurity content, and numerous intercalated non-saline insoluble (glauberite, anhydrite, mudstone, shale, etc.) (LIU et al., 2015). This feature made it difficult to build storage caves in these salt formations. Still, the work developed by YIN et. al (2020) showed that China was successful in the construction and operation of underground natural gas storage caverns through underground gas storage (UGS) in Jintan, in addition to other cavern projects of this type still under development. These experiments showed a confidence in storing hydrogen as well, as shown by LIU et al. (2020) in their work studying the feasibility of building underground hydrogen storage (UHS) caverns in Jiangsu province, China.

In Brazil, the strategic storage of hydrocarbons is still under study; however, the main challenge (and impediment) in opening and maintaining an offshore cavern has been the high cost involved in mobilizing equipment for deep water, dissolution mining is currently adopted in basins of the Recôncavo (Matarandiba Island) (FIRME et al., 2019).

2.1 PROS AND CONS OF USING SALT CAVERNS

Salt caverns were first used for the storage of fossil fuels such as natural gas, crude oil and petroleum products, later their use extended to the storage of compressed air and hydrogen, in addition, there is also the use them as a location for

the dismantling of toxic or nuclear waste. The ability to store large amounts of fluids and gases under high pressures is just one of the many advantages offered by these cavities, it also stands out:

- The favorable mechanical properties of salt, which allow the construction and operation of extremely large stable cavities for long periods of time, are also completely impermeable to gases. Furthermore, the salt is inert towards gases and hydrocarbons, the exploration phase is usually much less labor intensive compared to storage in aquifers since many salt structures are already known from oil and gas exploration and the investigation of salt as a raw material in itself (DONADEI & SCHNEIDER, 2016);
- High injection and withdrawal rates, multicycling capability (eCORP International, 2021);
- Flow rates can be high and can be brought into operation and increased to full flow quickly, they are better for covering daily demand spikes and short-term trade rather than long-term seasonal storage (MOKHATAB et al., 2019);
- Justifiable economics through dissolution mining, low working gas, high delivery capacity, low investment, low maintenance and operation cost, low energy needed during injection and production cycles, salt accessibility worldwide (HABIB, 2019).

Despite presenting itself as a globally accepted and propagated environmental solution, some factors can be considered negative, they are:

- Due to the sheer size of these caverns, especially the larger ones, they can take several years to be completely built;
- The construction of an underground salt cavern requires a prior exploration phase which can be time-consuming and costly;
- During the process of opening these cavities through dissolution mining, large volumes of brine are generated, which must be disposed of safely and properly, this is an issue that can often become an impasse during construction and operation;

- The volume of each cave has practical and geological limitations, higher operating cost due to the corrosive environment (eCORP International, LLC).

2.2 METHODOLOGIES FOR DISSOLUTION

For the opening of the cavity in the salt rock, the leaching technique is used, better known as dissolving mining. On land, fresh water is the fluid used in the dissolution process while in the offshore environment this fluid is the seawater itself, differences apart, the dissolution methodology is the same in both environments. As an initial step, before leaching, it is necessary to open a well through the salt layer.

The wells are constructed considering both subsequent activities: construction of the salt cavity and operation of the hydrocarbon stock, thus, the structural design of the wells must be reinforced (casing), as well as the diameter necessary to develop both activities (COSTA, 2018). In addition to these should be considered also the arrangement of wells, addressed below.

2.2.1 Well Arrangements for the Construction of Caverns

Among the possible arrangements for disposing of caverns in evaporitic rocks, the following stand out:

A cavern with a single well: The simplest and most common, the construction of the cavern takes place through the gradual leaching of the salt layers, Figure 1a.

Two caverns with a single well: In this type of configuration there are two layers of salt separated by a thick non-saline rock, being more appropriate for gas storage constructions, Figure 1b.

A cavern with two wells: Two wells drilled adjacently and connected in the same salt layer. One well for water injection and another for the return of the brine produced, Figure 1c.

Figure 1 – Well arrangements for the construction of caverns

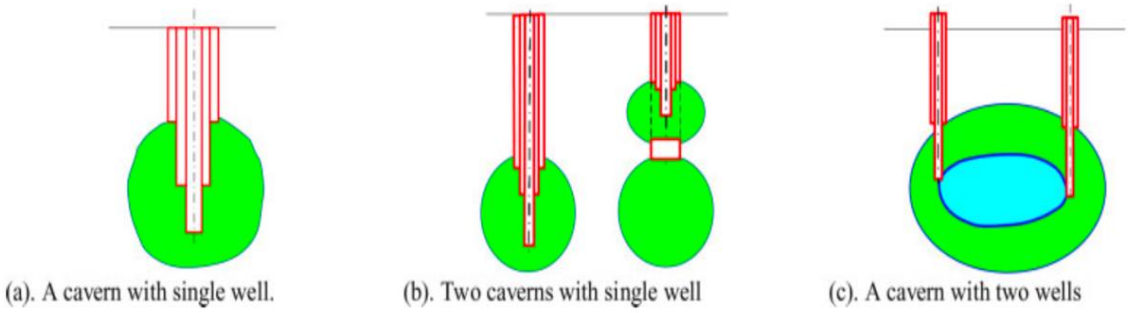

Source: Tian et al. (2010).

2.2.2 Water dissolution and circulation methodologies

The dissolution of the salt rock for opening the cavern can be based on the following configurations:

Dissolution from bottom to top: in this method two ways are presented to control the geometry of the cavern during its construction. The first method pulls the water injection pipe gradually and fixes the drain pipe (Figure 2a1) and the second method fixes the leaching pipe and moves the drainage pipe (Figure 2a2). It is the most widely used dissolution method in cavern construction.

Dissolution from the top to the bottom: in this method, first a small cavity is constructed at the top of the salt layer and then the salt is dissolved, forming the salt cavern (Figure 2b).

Integral dissolution: this is due to the combination of the two previous methods (Figure 2c).

Figure 2 – Dissolution of a) bottom to the top; b) from the top to the bottom; c) integral

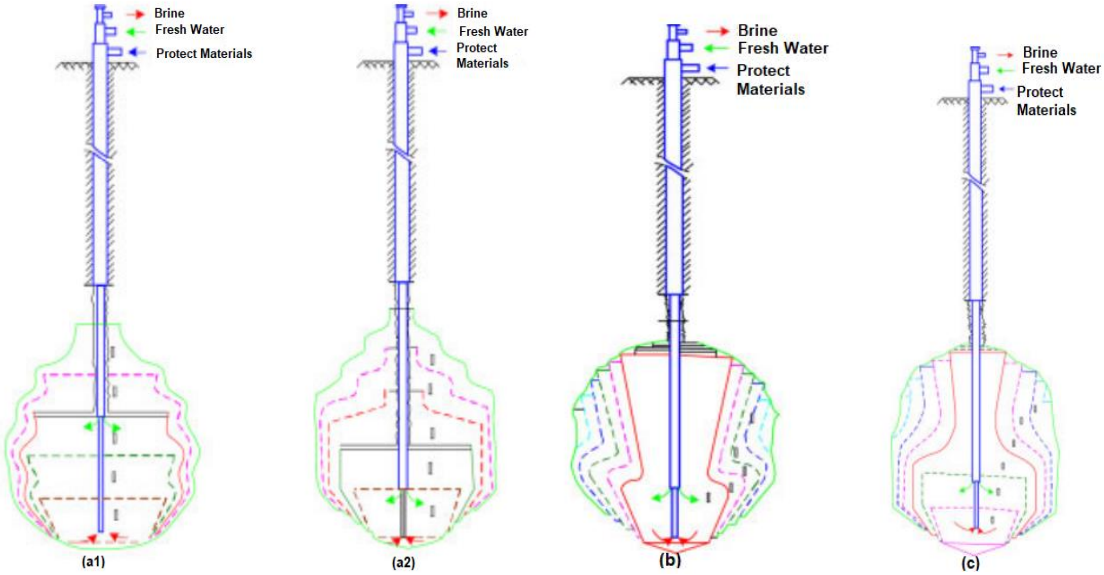

Source: Adapted from Tian et al. (2010).

For injection and consequent circulation of water inside the cavern are considered two methods:

Reverse Circulation: in this method fresh water or sea water, will depend on the environment, is injected at the top of the cavern and the brine is extracted at the bottom of the cavern. Generally, there is a cavern in inverted cone-shaped (Figure 3a). This method has the advantages of allowing the increase of brine density and improving the efficiency at construction speed on the other hand makes it difficult to control the shape of the cavity, stability and protection of the top of the cavern.

Direct Circulation: in this method the water is injected into the bottom of the cavern and the brine is extracted from the top of the cavern. Typically, this configuration allows the generation of a pear-shaped cavern (Figure 3b). The advantages of reverse circulation method are the disadvantages of the direct method, as well as the disadvantages of reverse are the advantages of the direct method.

Figure 3 – Reverse and direct circulation processes for the opening of salt caverns

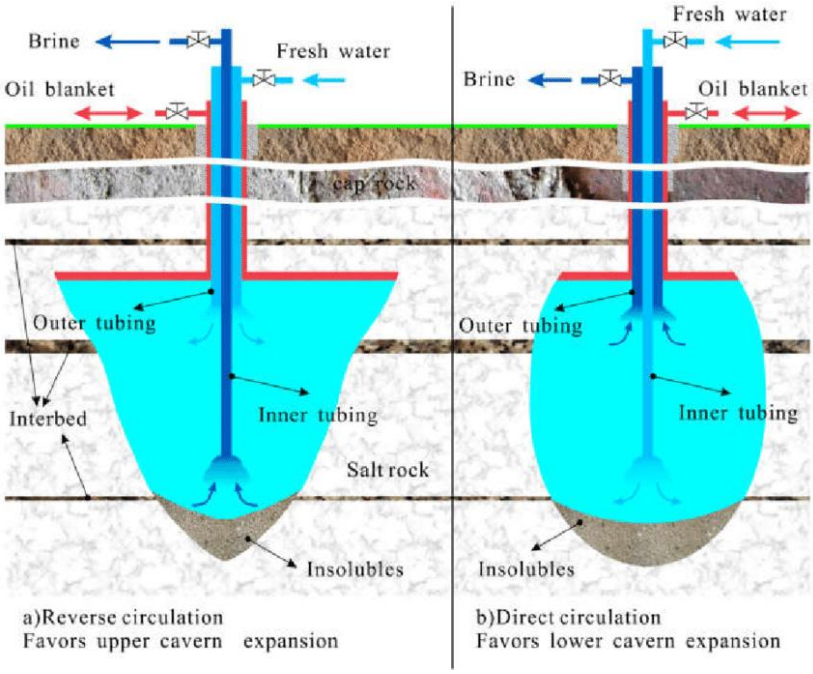

Source: Ge et al. (2019).

2.3 CAVERN CONSTRUCTION

In order to find more efficient ways to build underground caverns in salt rocks, different authors have carried out studies in the area. Efforts were mainly directed towards the leaching phase, one of the most time-consuming and important. Laboratory tests, mathematical and numerical models were developed with the aim of reducing the time spent in this phase and consequently optimizing the cavern's development.

2.3.1 Experimental Tests

The vast majority of laboratory tests produced studied the process of dissolution of the salt rock.

SMIRNOV et al. (2002) described an experimental method to determine the dissolution speed coefficient of salt rock, under the convection process in rock sections obtained by sampling in the well, the statistical processing of the results showed that the dissolution rate coefficients are smaller for rock salt interspersed with other rocks in layers, than the pure deposits of that salt.

JINPING et al. (2008) presented a fast speed dissolution tool in the salt cavern, the principles of this instrument were presented based on the cavitation jet theory. Field application of this tool shows that it can increase the rate of leaching of salt rock over time, it can also drive insoluble materials from the bottom of the cavern to the floor and increase the volume of the cavern.

Another study also under the same aspect was presented by WEISBROD et al. (2012), where laboratory tests were carried out to study the dynamics and dissolution rate of natural salt rocks (halite). These rocks were subjected to the flow of unsaturated solution to analyze the dynamics of expansion of the cavities due to dissolution. To analyze the geometries of these cavities, these authors used computed tomography.

It was also found that for specific values of injection flows, the rocks start to form preferential flow paths, however for values below these, the flow through the sample may cease due to salt precipitation inside the pores.

LIU et al. (2016) studied the mechanisms of salt dissolution under the effect of gravity using a dynamic dissolution test, in which rock cores were subjected to dissolution at different flow rates. From the brine produced, the amount of dissolved salt was evaluated numerous times for each sample.

JIANG et al. (2016) performed laboratory tests based on an analysis of degrees of freedom, modeling the construction of a real cave with a salt mold that could represent a salt core obtained from drilling. In the experiments, a method was proposed by the authors to determine the positioning of the oil-water interface and the shape of the cavern, based on the conductivity characteristics of the saturated brine.

The results of the experiments showed that when the location of the oil blanket is close to the intermediate layer, the rate of construction or leaching decreases because the presence of the intermediate layer reduces the effective dissolution area and hinders the convection and diffusion of the brine.

More recently JIANG et al. (2021) performed a series of physical simulation tests of water-dissolving caverns using two-well-vertical (TWV) with gas blanket technology. Even at an early stage, this technology has the advantages of achieving a larger cavern volume, clean brine, large water flow and great economic benefits.

The survey results indicated that the technology of the TWV cave construction with gas blanket is promising for brine leaching and energy storage cavern construction and it is also worth further study.

2.3.2 Mathematical and Numerical Models

In line with experimental tests, several mathematical and numerical models were also developed. In the work of DURIE & JESSEN (1964), the authors proposed, in addition to laboratory tests, a mathematical model that describes the dissolution process as a function of water salinity at any point on the vertical surface of the salt.

They concluded that, under low injection rates, dissolution by natural convection and forced convection is very similar as the induced flow does not significantly contribute to the rate of salt removal. Furthermore, under the laminar flow regime, the dissolution rate is strongly affected by the salinity of the water and not the injection rate. Another point is that the rate of salt removal is not very different in forced convection and in natural convection.

After this work, DONAT (1972) used a numerical model to simulate the process of building salt caverns for gas storage. In his modeling, the author simulated the construction of a real reservoir located in France.

This reservoir was located at a depth of 1400 m and had two cavities with volumes corresponding to 90,000 and 125,000 m^3, in which the gas was stored in operating pressure cycles ranging from 80 to 220 kgf/cm^2.To control the dissolution at the top of the cave, fuel oil was used, whose contact zone with the brine is determined by radioactive tracers

Shortly thereafter, SABERIAN (1974) presented a generalized numerical model for predicting cavity dissolution as a function of time and other physical parameters, such as velocity, radius and dissolution rate, in addition to including simulations with forward and reverse circulation.

Years later, KUNSTMAN & URBANCZYK (1990) developed a mathematical model that takes into account the sedimentation of insoluble materials, as well as the volumetric brine concentrations. Furthermore, this model is able to predict the course of dissolution by direct and reverse circulation, with or without the presence of an oil layer on top of the cavern.

KAZARYAN et al. (2007) discussed the opening of caverns by dissolution of salt rocks of limited thickness, interspersed with insoluble layers, mainly anhydrite and dolomite, with a few meters of thickness, in the region of Irkutsk, Russia.

The development of the cavern was numerically simulated by these same authors through the computer codes SALGAS (SMRI) and Rock Salt Dissolution at Underground Gas Industry (RSDUGI – Podzemgazprom), where SALGAS considers only the vertical stratification of the brine and, so that's why, they used also, the RSDUGI code to simulate the development of caverns by dissolution through vertical wells.

The excavation for the construction of caverns results in the emergence of deflecting stresses, due to the disturbance of the stress balance "in situ".

ALKAN et al. (2010) indicate that the dilation limit is a critical point for the opening and/or formation of microcracks in a crystalline rock subjected to deflecting stresses. They showed that pore volume and permeability decrease first in the compression phase, and assume a minimum value at the dilation limit. This article performs the evaluation and comparison of numerical approximations used for the prediction of the stress-expansion-permeability relationship in zones of excavation damage in saline rocks.

An increase in the number of publications on cavern construction has occurred in the last decade. Many of these works were published in the city of Maulo in the Jintan region of China. Among these, HUANG & XIONG (2011) studied the influence of intermediate layers on cavern stability and on the probable loss of stored natural gas, due to leakage along the interface.

LI et al. (2016) proposed a mathematical model to predict the form of accumulation of insoluble sediments during leaching, in addition to depositing at the bottom of the cave, these sediments contribute to reducing the useful storage volume of the cave.

These authors also performed laboratory tests to determine the properties that affect the form of accumulation of insoluble particles. They found that this is mainly affected by the coefficient of expansion of the insolubles in the brine, the amount of insoluble components present in the salt rock, and the height of the cave wall.

Under normal conditions, less soluble materials are precipitated upon dissolution of the salt, and the geometry and texture of these residues provide clues

to the time, rates and processes of dissolution. These deposits include salt, anhydrite, gypsum and calcite (HOVORKA, 2000).

YANG & LIU (2017) developed a mathematical model to simulate the dissolution of rock salt in the construction of the cavern, whose solvent is injected under a dynamic flow condition. They wanted to observe with a simulation, the factors that influenced the process of dissolution of the walls of the salt rock and the speed with which the rock dissolved, the model was validated through laboratory tests of the dissolution of salt rock.

YANG & LIU (2017) also used numerical simulations to understand the factors influencing the process of dissolution of the salt rock walls and the velocity with which the rock dissolved. The model was compared with laboratory tests of salt rock dissolution, obtaining a good correlation between numerical simulation and laboratory tests.

YANG et al. (2017) presented a proposal for an analytical solution of a differential equation to calculate the dissolution rate of salt rocks subjected to an instantaneous diffusion process. The dissolution parameters are obtained from the dissolution kinetics built with laboratory tests, the results showed a fit between the numerical model and the experiment of the concentration of salt in water in relation to time.

Seeking to understand the shape of the cavern and guarantee its safety, the same authors, LI et al. (2018) developed a mathematical model to predict cavern behavior during leaching into insoluble salt formations.

WANG et al. (2018) presented a mathematical model to predict the parameters of the debrining for a salt cavern used for gas storage based on the principle of pressure equilibrium and the change in the dynamic characteristics of the gas/salt interface.

BROUARD et al., (2018) presented a routine that inserted the numerical approach in 3D to their LOCAS software. Brouard Consulting developed the LOCAS salt cavern modeling software that is capable of coupling cave thermodynamics and the geomechanics of the salt/rock domain.

More recent salt rock dissolution technologies were also addressed, in addition to the TWV technology studied by JIANG et al. (2021), another technology was used in the construction of gas caverns, WAN at al. (2019) applied basic principles of the Navier-Stokes equation and established a new 3D mathematical

model which included flow and mass transfer and boundary movement for two-well-horizontal (TWH) salt cavern construction.

In addition to a mathematical model for the construction of underground TWH caverns, the authors WAN at al. (2019) developed a new computer code program TWHSMC (Two-well-horizontal solution mining cavern) for solution mining and presented numerical simulations. The results of the cavern shapes simulation by program were compared with the experimental ones, indicating that the model successfully and accurately predicts the cavern shape and demonstrates its reliability and applicability.

Underground TWH caverns in salt rock have high construction efficiency and large usable volumes in addition to providing an ideal space for large-scale natural gas storage.

Years later, WAN et al. (2021) performed a set of numerical simulations, based on the original TWHSMC V2.0 (two-well horizontal solution mining cavern V2.0) dissolution mining numerical simulation program to analyze the influence of tubing/oil-blanket lifting on construction and geometries of two-well-horizontal salt caverns. These cavern types are an ideal storage medium for large-scale energy storage, with large usable volumes and high construction efficiency.

Although the storage of energy sources and waste in general in underground caverns is a very widespread technology, given the number of studies carried out in the area, in recent years, there has been a trend towards the inclusion of the various phenomena that govern the process of opening these cavities by dissolution.

This increase was due to the possibility of using new computational technologies that allow the simulation of more complex processes, involving several coupled phenomena, as well as the development of new dissolution techniques.

In this sense, to analyze the dissolution process in an underground cavern, the present work developed simulations utilizing the SALGAS software.

The next chapter explains better this finite difference code as well as its main characteristics.

3 CAVERNS OPENING WITH THE SALGAS

This chapter discusses concepts, characteristics and highlights the main advantages and limitations of the SALGAS software, in addition to presenting the equations that govern the calculation of input data for the program.

The representation of possible scenarios of opening an underground cavern in salt rock by dissolution was possible through the SALGAS software, written in FORTRAN in the mid 1970's. This finite difference code developed by the Solution Mining Research Institute (SMRI) to simulate the dissolution of sodium chloride salt by water, optionally simulates the hydraulic properties and power requirements of the mining system.

Furthermore, it is also possible to simulate the properties of the blanket, fluid bed used to protect the roof of the cavern from possible upward dissolving. This software has been validated through laboratory experiments and from data from caverns in salt domes on the US Gulf Coast (EYERMAN et al. 2008).

3.1 ADVANTAGES AND LIMITATIONS

Originally developed to meet the demands of the mining sector, this code could also help other areas, such as the oil industry. Among one of its main advantages is the possibility of generating the following data through simulations, cavern volume, amount of insolubles, salt production and pipe head loss, in addition to the costs of the production pumping system, other benefits are:

- Input and output of data in the program can be in British and Metric units;
- Possibility of adjusting the blanket level;
- To solve the problem, use reactive transport;
- Uses the finite difference numerical method;
- It is based on the turbulent flow hypothesis;
- During the simulation or when performing a "restart", it is possible to change the mining direction (direct to reverse or vice versa);
- Possibility of restarting the simulation to change input parameters.

Despite all the advantages presented, the main limitation of this program is to simulate offshore scenarios, the field of action is better represented for onshore scenarios. Other disadvantages are:

- Considers only the vertical stratification of the brine;
- When referring to the input parameters in the program, with the exception of the specific density of the injection fluid, all other input parameters are relative to production data;
- Regarding the injection points, during the simulation only one injection point is possible, with the possibility of changing the position by means of a “restart”;
- Similar to the previous topic, during the simulation only one production point is possible, with the possibility of changing the position by means of a “restart”.
- The generated mesh is a one-dimensional mesh limited to 200 cells, previously it was 60 cells.

3.2 EQUATIONS FOR THE CALCULATION OF SALGAS INPUT DATA

The following input parameters for SalGas are obtained through mathematical equations, they are: specific density of the injection fluid, specific density of the produced brine, salt dissolution factor and injection pressure.

The specific density of saline injection solution is the ratio between the density of the fluid and the density of pure water at a temperature of 4°C and a pressure of 1 atm.

The density of the saline solution to be injected, ρ_b (kg/m³), according to ATG (1986) is a function of temperature, T (Kelvin), fluid pressure, P (bar), and mass salt concentration, c_b, being determined by eq. (1):

$$\rho_b\,(P, T, c_b) = \frac{1000}{v\,(P,T,c_b}) \tag{1}$$

Where v (P,T,c_b) is the specific volume of the injection fluid (cm³/g) and can be calculated using eq. (2):

$$v(P,T,c_b) = A(T) - P'B(T) - P'^2C(T) + c_bD(T) + c_b{}^2E(T) - c_bP'F(T) - c_b{}^2P'G(T) - \frac{1}{2}c_bP'H(T) \quad (2)$$

Being P' = P/0.981, P in bar, and A,B,C,D,E,F,G,H functions of the injection fluid temperature. These functions are given by eq. (3):

$$\varphi = \varphi_0 + \varphi_1 T + \varphi_2 T^2 + \frac{\varphi_{11}}{T} + \frac{\varphi_{12}}{T^2} \quad (3)$$

With the coefficients used to calculate the functions A,B,C,D,E,F,G and H given in tab. (1):

Table 1 – Coefficients for calculating functions A,B,C,D,E,F,G and H

	φ_0	φ_1	φ_2	φ_{11}	φ_{12}
A	5.916365	-1.035794×10^{-2}	9.270048×10^{-6}	-1127.522	100674.1
B	5.204914×10^{-3}	-1.0482101×10^{-5}	8.328532×10^{-9}	-1.1702939	102.278
C	1.18547×10^{-8}	-6.599143×10^{-11}	0	0	0
D	-2.5166	1.11766×10^{-2}	-1.70552×10^{-5}	0	0
E	2.84851	-1.54305×10^{-2}	2.23982×10^{-5}	0	0
F	-1.4814×10^{-3}	8.2969×10^{-6}	-1.2469×10^{-8}	0	0
G	2.7141×10^{-3}	-1.5391×10^{-5}	2.2655×10^{-8}	0	0
H	6.2158×10^{-7}	-4.0075×10^{-9}	6.5972×10^{-12}	0	0

Source: Atg (1986).

The density of pure water, ρw (kg/m³), according to PATTERSON & MORRIS (1994), is a function of temperature, T (ºC), fluid pressure, P (MPa), and given by equation (4):

$$\rho_w(T) = \rho_w^0 \left[1 + \frac{(T+a_1)^2(T+a_2)}{a_3(T+a_4)}\right][1 + (b_1 + b_2T + b_3T^2)(P - P^{ref})] \quad (4)$$

Where:

ai and bi are constants; P^{ref} = 1 atm = 0.101325 MPa.

Pure water parameters are shown in tab. (2):

Table 2 – Pure water parameters

$\rho_w^0 = 999.972\ \text{kg/m}^3$	$a_4 = 69.34881\ ^\circ\text{C}$
$a_1 = -3.983035\ ^\circ\text{C}$	$b_1 = 5.074\times10^{-4}\ \text{/MPa}$
$a_2 = 301.797\ ^\circ\text{C}$	$b_2 = -3.26\times10^{-6}\ \text{/MPa-°C}$
$a_3 = 522{,}528.9\ ^\circ\text{C}^2$	$b_3 = 4.16\times10^{-9}\ \text{/MPa-°C}^2$

Source: Patterson & Morris (1994).

All the equations shown above and also the specific gravity of saline injection solution are built into the Toolbox provided by SMRI and can be calculated in the Fluids>Brine>Under-Saturated Brine Calculator tab, as shown in fig. (4):

Figure 4 – Under-Saturated Brine Calculator tab

Source: Brouard (2008).

Another input parameter that needs mathematical development is the specific density of the produced brine, which is the ratio between the density of the fluid with the saturation concentration and the density of pure water at a temperature of 4°C and pressure of 1 atm.

The mass salt concentration present in the saturated brine, c_b^{sat}, depends on pressure, P (MPa) and temperature, T (°C). According to ATG (1986) its shape is defined by eq. (5):

$$c_b^{sat}(P,T) = a_0 + a_1 T + a_2 T^2 + bP \quad (5)$$

Where ai and bi are constants, whose values are in tab. (3):

Table 3 – Constant values a_i e b_i

a_0	a_1	a_2	b
0.26291	0.7448×10^{-4} /°C	0.1252×10^{-5} /°C²	7.5×10^{-5} /MPa

Source: Atg (1986).

The equation for the density of pure water has already been demonstrated above. Both it and the salt concentration equation and the specific gravity of the produced brine are built into the Toolbox provided by SMRI and can be calculated in the Fluids>Brine>Saturated-Brine Calculator tab, as shown in fig. (5):

Figure 5 – Saturated-Brine Calculator tab

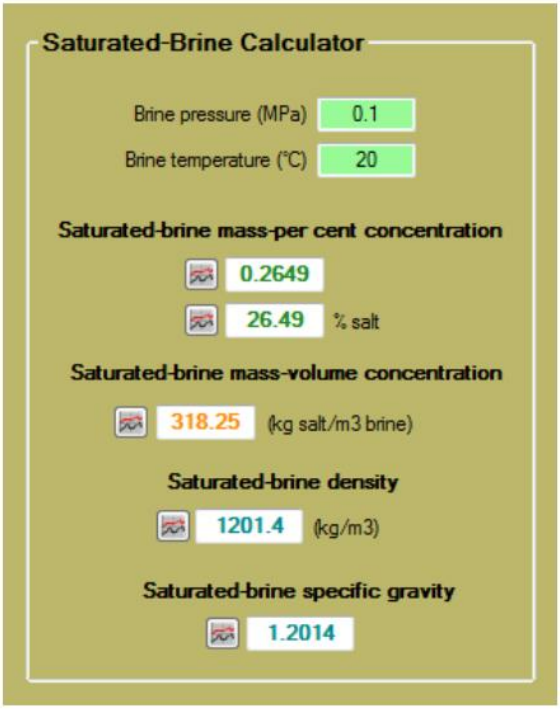

Source: Brouard (2008).

The third input parameter that requires mathematical calculation to be determined is the dissolution factor.

According to SABERIAN (1983) it is possible to obtain the dissolution rate of a brine, m_T (cc/cm²/min x 10³), for different temperatures and salinities, as a function of the specific density of the brine, ρ (-), of the reference temperature, T_0 (°F), and the initial production temperature, T (°F), according to eq. (6):

$$\dot{m}_T = 0.22(1.2019 - \rho)^{1.42}\, exp\,[0.0119\left(\frac{\rho-1}{1.2019-\rho}\right)^{0.2}\Delta T \quad (6)$$

As in SalGas the reference temperature is 75°F and all the simulations performed are isothermal fixed for this temperature, the input data instead of being the dissolution rate is the dissolution factor which is the exponential term of equation (3.6) for an ideal salt (T_0=75°F and ρ=1.20).

The dissolution factor, DF, is an input parameter in SalGas that corrects the dissolution rate by compensating between a 75°F isothermal simulation of an “ideal salt”, which would generate a brine with the maximum specific gravity accepted by the software. = 1.2, and the simulation that actually needs to be done, with temperature and specific densities different from the ideal. Given by eq. (7):

$$DF = exp\, exp\,[0.03 * (T - 75)] \quad (7)$$

Where:

T = Initial production temperature (°F).

The injection pressure, P (MPa) is the difference between the pressure of the fluid to be injected, P_1 (MPa) and the pressure of fluid in the massive, P_2 (MPa). With P_2 known, the Bernoulli equation is used to find P_1, through eq. (8):

$$\frac{P_1}{\gamma} + \frac{v_1^2}{2g} + z_1 = \frac{P_2}{\gamma} + \frac{v_2^2}{2g} + z_2 \quad (8)$$

Where:

g = gravity acceleration (m/s²);

P = pressure (Pa);

v = velocity (m/s);

z = height (m)

γ = specific weight (N/m^3)

z_1=z_2; v = flow/area; γ = ρg.

Given the injection pressure, P (MPa) it is possible to determine the pressure at the height of each injection valve, P_i (MPa) by eq. (9):

$$P_i = \frac{H_i}{P} \tag{9}$$

Where:

Hi = injection valve height.

As simulations are performed with different flow rates for the same injection valve height, the SalGas input pressure will change according to the flow variation at that height, and can also be determined by the Bernoulli Equation through eq. (8).

4 PCA AND THE USE OF THE PAST SOFTWARE

In this chapter, the definition, characteristics, main advantages and limitations and the mathematical development of the PCA statistical tool are discussed, in addition to the use of the PAST software.

In addition to simulating possible scenarios of opening an underground cavern in salt rock by dissolution with the SALGAS software, it was also possible through this research to analyze the data from the simulations considering multivariate data analysis, for this the statistic tool PCA (Principal Component Analysis) was used.

The PCA was originally proposed by Karl Pearson in 1901 and later by Hotelling (1933) and Loève (1963), also known as the Hotelling Transformation or Karhunen-Loève Transformation.

4.1 DEFINITION AND CHARACTERISTICS

When a large amount of complex data is available and the intention is to infer the greatest amount of relevant information from them, multivariate statistical analysis is used. This includes, therefore, all statistical techniques that simultaneously analyze multiple measurements on individuals, objects or parameters under investigation.

HAIR et al. (2009) believe that multivariate analysis does not have a rigid definition, and can include both techniques with many variables and truly multivariate techniques, according to them, some authors establish that the objective of multivariate analysis is to measure, explain and predict the degree of relationship between variables statistics (weighted combinations of variables).

Within the multivariate techniques, the PCA technique was chosen in the present work, due to the proposal of the tool. Considering the good amount of variables obtained by the simulations, this technique allows analyzing the interrelation between them, explaining them in terms of their variability (variance) and their contribution to the process of opening the salt cavity by dissolution.

In this method there is a linear transformation that allows a set of originally correlated variables to be converted into a set of independent variables called principal components (PC). The objective, therefore, of the technique is to find a way

to condense the information contained in several original variables into a smaller set of statistical variables, keeping a minimum loss of information.

Principal Component Analysis eliminates redundancy between data and rearticulates them in a new space where each axis, orthogonal to each other, represents a principal component, which are produced by linear combinations of the original variables. The number of principal components is therefore equal to the number of original variables.

4.2 ADVANTAGES AND LIMITATIONS

Among the main advantages of the PCA technique, the following stand out:

- The practicality and ease of implementation;
- Be a purely statistical technique;
- Removing the multicollinearity of the variables, as it allows transforming a set of original intercorrelated variables into a new set of uncorrelated variables (principal components) (HONGYU et al., 2015);
- Reduction in storage cost, as data is condensed into a smaller set of variables;
- Widely disseminated and used.

On the other hand, it has the following main disadvantages:

- In general, information is lost during the process, due to the reduction in the number of variables;
- It is not recommended when there are more variables than sample units;
- It doesn't always work, even with the transformation it's still great.

4.3 MATHEMATICAL DEVELOPMENT

Is known that Principal Component Analysis performs a linear transformation to convert a set of original variables dependent on each other into a set of independent variables capable of explaining the new set of data in terms of their variability. In short, this process takes place as follows: establish a set of X variables and n observations, assemble a matrix with these data; obtain the average and standardize the data; calculate the covariance matrix; determine the eigenvalues and eigenvectors and determine the principal components (KOHLER, 2013).

First, a population π is taken, in which 'p' characteristics of 'n' observations are considered. To represent the characteristics, the variables X1, X2, ..., Xp are used. From this set of n x p measurements, a matrix of data **X** (n x p) is generated:

$$X = \begin{bmatrix} x_{11} & \cdots & x_{1p} \\ \vdots & \ddots & \vdots \\ x_{n1} & \cdots & x_{np} \end{bmatrix}$$

The next step is to calculate the average $\underline{X}$ and normalize the data. As the characteristics are normally observed in different measurement units, according to REGAZZI (2000) it is convenient to standardize the variables. The standardization can be done with zero average and variance 1, from the application of eq. (10):

$$\boldsymbol{z_{ij} = \frac{x_{ij} - \underline{x_j}}{s(x_j)}, i = 1, 2, \ldots, n \; e \; j = 1, 2, \ldots, p} \qquad (10)$$

Where:

z_{ij}: standardized values,

x_{ij}: samples for i = 1,2, ..., n and j = 1,2, ..., p

$\underline{\boldsymbol{x_j}}$: estimative of the average of characteristic j,

$s(x_j)$: standard deviation of characteristic j.

The fourth step is to calculate the covariance matrix 'S', which represents the independence structure between the variables of the data matrix, as well as the correlation matrix 'R'. In practice, it is difficult to understand this structure through the variables X_1, X_2, ..., X_p. Thus, the objective of principal component analysis is to transform this complicated structure, represented by variables X_1, X_2, ..., X_p, into another structure represented by uncorrelated variables Y_1, Y_2, ..., Y_p and with ordered variances, so that it is possible to compare individuals using only the Y_{is} variables that present greater variance (VARELLA, 2008).

The matrix S is square symmetric, of the order 'p x p'.

$$S = \begin{bmatrix} var(x_1) & cov(x_2x_1) & cov(x_1x_2) & \ldots & var(x_2) & \ldots & cov(x_1x_p) & cov(x_2x_p) & \vdots \\ \vdots & & \ddots & \vdots & cov(x_px_1) & cov(x_px_2) & \ldots & var(x_p) & \end{bmatrix}$$

With standardization we get a **Z** data matrix.

$$Z = \begin{bmatrix} z_{11} & z_{21} & z_{12} & \dots & z_{22} & \dots & z_{1p} & z_{2p} \\ \vdots & \vdots & \ddots & \vdots \\ z_{n1} & z_{n2} & \dots & z_{np} \end{bmatrix}$$

The fifth step is to determine the eigenvalues and eigenvectors. For this, equation (11) is solved, which is the characteristic equation of the matrix R or S:

$$det\ \boldsymbol{det}\ [\boldsymbol{R} - I] = \mathbf{0}\ \boldsymbol{ou}\ |\boldsymbol{R} - I| = 0 \quad (11)$$

If the matrix R does not present any column that is a linear combination of another, the equation will have real and distinct roots 'p', called eigenvalues, they are λ_1, λ_2, ..., λ_p, where:

$$\lambda_1, \geq \lambda_2, \dots, \geq \lambda_p.$$

For each eigenvalue λ_i there is an eigenvector $\tilde{e_i}$:

$$\tilde{e}_i = \begin{bmatrix} e_{i1} & \dots & e_{ip} \end{bmatrix}$$

Finally, having found the eigenvalues and eigenvectors pairs (λ_1,e_1), (λ_2, e_2), ..., (λ_p, e_p), the i-thus principal component is defined by eq. (12):

$$Y_i = e_{i1}X_1 + e_{i2}X_2 + \cdots + e_{iP}X_P \quad (12)$$

In PCA, the eigenvalues of the covariance matrix correspond to the variance of the transformed variables, eq. (13):

$$\boldsymbol{var}(Y_i) = \lambda_i \quad (13)$$

In addition, the first principal component represents the one with the highest original variance of the data, the second represents the second with the highest variance, and so on, until the last component. That is, for each subsequent component, a residual variance remains, which is getting smaller and smaller.

Another important observation is that these components are orthogonal to each other, so they are not correlated, eq. (14):

$$\boldsymbol{cov}(Y_i, Y_j) = 0 \tag{14}$$

When one intends to quantify the importance of a principal component, the concept of contribution C_i of each principal component Y_i is used, expressed in percentage, the contribution of each component represents the percentage of the total variance of the data that each one of them retains, eq. (15):

$$C_i = \frac{var(Y_i)}{\sum_{i=1}^{p} var(Y_i)}\, x\, 100 = \frac{\lambda_i}{\sum_{i=1}^{p} \lambda \mathrm{i}}\, x\, 100 = \frac{\lambda_i}{trace\ (S)}\, x\, 100 \tag{15}$$

Where: trace (S) corresponds to the sum of the main diagonal elements.

In this model of k principal components, the sum of the first k eigenvalues represents the proportion of information retained in the reduction of p to k dimensions, based on this it is possible to determine the number of components that must be retained. In many cases, models that explain at least 80% of the total variation are adopted (JOHNSON; WICHERN, 1998).

When the intention is to know the degree of influence that each variable X_j has on the Y_i component, the correlation between each X_j and the Y_i component being interpreted is used, taking as an example the correlation between X_j and Y_1 through the eq. (16):

$$\boldsymbol{Corr}(\boldsymbol{X_j Y_1}) = \sqrt{\lambda_1}.\frac{a_{1j}}{\sqrt{var(X_j)}} \tag{16}$$

The influence of X_1, X_2, X_3, ..., X_n for the Y_1 component can be analyzed through the weight of each variable on the component, as follows in eq. (17):

$$w_1 = \frac{a_{11}}{\sqrt{var(X_1)}}, w_2 = \frac{a_{12}}{\sqrt{var(X_2)}}, \ldots\ w_p = \frac{a_{1p}}{\sqrt{var(X_p)}} \tag{17}$$

Where w_1 is the weight of X_1.

In addition to the concepts of contribution of each principal component and correlation between variable and component, another widely used concept is the score. The scores are the projections of the samples in the direction of the principal components, defined by equation (12).

4.4 PAST SOFTWARE

In general, there are several software that perform the statistical treatment of data, PAST was chosen for its practicality, ease of plotting data and obtaining results, in addition to the simple and dynamic interface. It is free software, freely available to perform a variety of scientific data analysis.

In addition to performing principal component analysis, it also has functions for other univariate and multivariate statistical analyses, data manipulation, plotting, ecological analysis, time series and spatial analysis, morphometry and stratigraphy. Data entry is spreadsheet type and many of its functions are paleontology and ecology specific and not found in more extensive standard statistical packages (HAMMER, HARPER, & RYAN, 2001).

PAST also includes fourteen case studies (data files and exercises) that illustrate the program's use for paleontological problems, making it a complete educational package for courses in quantitative methods.

5 METHODOLOGY

In this chapter, the solution mining scenarios for the opening of the underground cavern in salt rock are discussed with the description of the input data for the SALGAS software and for the PAST software.

Two hypothetical scenarios were considered for the study of the opening of an underground cavern in salt rock by dissolution, scenario D where water was injected at the bottom of the cavern and the brine was extracted from the top of it, through the so-called direct circulation method, and the scenario R where water was injected at the top of the cavern and the brine was extracted from the bottom of the cavern, in the so-called reverse circulation method. In tab. (4) the respective injection and production depths are presented for the considered scenarios and in fig. (6) their schematic representation.

Table 4 – Injection and Production depths for the proposed hypothetical scenarios

SCENARIO	ID (ft)	ID (m)	PD (ft)	PD(m)
SCENARIO D	3000	914,4	2500	762
SCENARIO R	2500	762	3000	914,4

Source: The Author (2022).

Figure 6 – Scenarios of salt cavern opening by dissolution

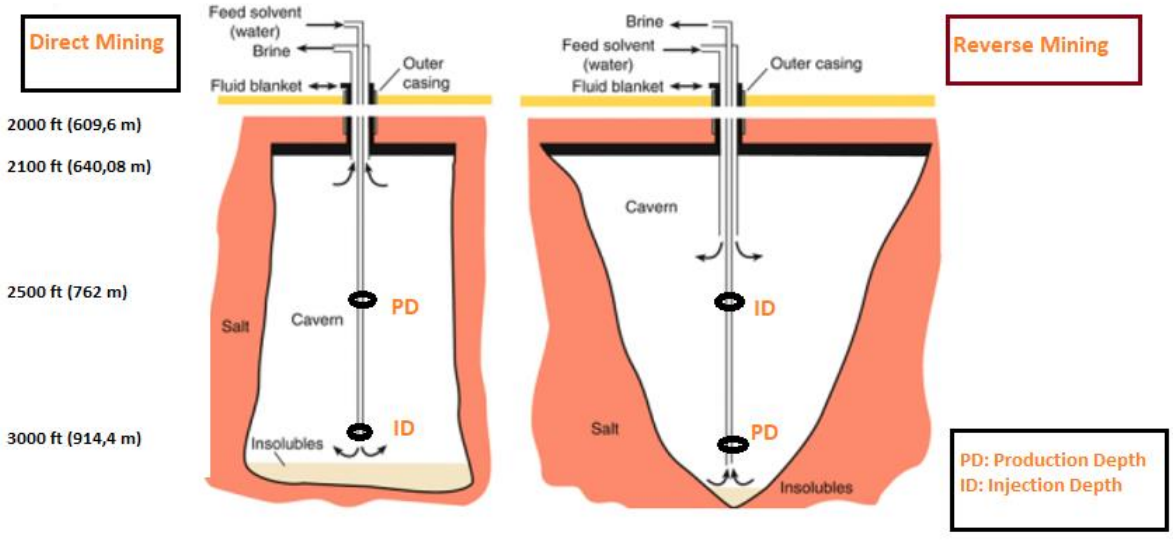

Source: Adapted from Warren (2006).

Both scenarios were based on example number 1 from the SALGAS Manual (EYERMAN, 2008). In this example, the development of a new cavern is started from a hole with a blanket, which moves up once, with 3% insolubles, considering a constant brine production rate and equal to 750 gpm (170,34 m³/h), the SALGAS base temperature of 75°F (23.9°C), depths of injection and production, 3000 e 2500 ft, respectively, and direct circulation method, during 120 days. The hydraulic model has a short section of surface piping and divides each of the piping lines into two sections, as can be seen in fig. (7).

Figure 7 – Initial geometry of Example 1

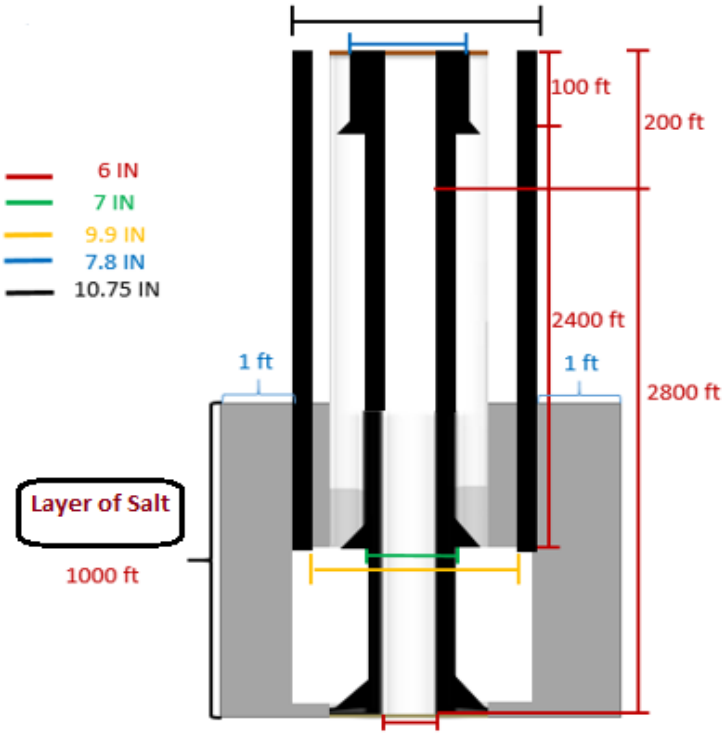

Source: The Author (2022).

From this base situation, new simulations were obtained in this study by varying the injection temperature, the brine production rate, and also considered the reverse circulation method. The diameters of the external and internal piping were the same as those considered in the example, respectively 10¾” (273.05 mm) and 7” (177.8 mm). The mining module was used together with the hydraulic module to simulate the dissolution of the rock by a fluid saturated in 4.05% of NaCl for 120 days.

5.1 INPUT DATA FOR THE SALGAS SOFTWARE

The tables 5 and 6 present the parameters that will be used in the SALGAS data input file for scenarios D and R respectively.

- SCENARIO D
- SCENARIO R

Table 5 – Input parameters for Scenario D

N	Injection Temperature (°C)	Injection Rate (m^3/h)	Injection Pressure (MPa)	Initial Brine Density	Injected Fluid Density	Salt Dissolution Factor
1	40	120	9.0500	1.196300	1.023930	1.25989419
2	40	200	9.1800	1.196400	1.024030	1.26016984
3	40	360	9.6700	1.196500	1.024230	1.26071911
4	40	400	9.8300	1.196600	1.024330	1.26099276
5	40	800	12.4200	1.197600	1.025430	1.26396075
6	40	1200	16.7400	1.199400	1.027130	1.26840665
7	60	120	9.0500	1.187400	1.014330	1.58798018
8	60	200	9.1800	1.187400	1.014530	1.59017741
9	60	360	9.6700	1.187600	1.014630	1.59126914
10	60	400	9.8300	1.187600	1.014730	1.59235636
11	60	800	12.4200	1.188700	1.015830	1.60403307
12	60	1200	16.7400	1.190500	1.017630	1.62214403
13	80	120	9.0500	1.179100	1.002830	1.67090079
14	80	200	9.1800	1.179100	1.002930	1.67697674
15	80	360	9.6700	1.179300	1.003130	1.68871982
16	80	400	9.8300	1.179400	1.003230	1.69440201
17	80	800	12.4200	1.180400	1.004330	1.75029718
18	80	1200	16.7400	1.182300	1.006130	1.82428703

Source: The Author (2022).

Table 6 – Input parameters for Scenario R

N°	Injection Temperature (°C)	Injection Rate (m^3/h)	Injection Pressure (MPa)	Initial Brine Density	Injected Fluid Density	Salt Dissolution Factor
1	40	120	7.5600	1.195700	1.023330	1.25822596
2	40	200	7.7100	1.195800	1.023430	1.25850574
3	40	360	8.2300	1.196000	1.023530	1.25878481
4	40	400	8.4100	1.196000	1.023630	1.25906319
5	40	800	11.2200	1.197200	1.024830	1.26235126
6	40	1200	15.9000	1.199000	1.026730	1.26737505
7	60	120	7.5600	1.186800	1.013730	1.58127404
8	60	200	7.7100	1.186800	1.013830	1.58240401
9	60	360	8.2300	1.187000	1.014030	1.58464903
10	60	400	8.4100	1.187100	1.014130	1.58576420
11	60	800	11.2200	1.188200	1.015330	1.59878792
12	60	1200	15.9000	1.190100	1.017230	1.61821655
13	80	120	7.5600	1.178500	1.002230	1.63097469
14	80	200	7.7100	1.178500	1.002330	1.63810134
15	80	360	8.2300	1.178700	1.002530	1.65174855
16	80	400	8.4100	1.178800	1.002630	1.65829672
17	80	800	11.2200	1.179900	1.003830	1.72622905
18	80	1200	15.9000	1.181900	1.005730	1.80920606

Source: The Author (2022).

Once the SalGas input file (*.sgi) has been assembled (appendix), proceed with running the case, as shown in the sequence of figures 8 to 11.

Figure 8 – Running the case at SalGas: Open the input file

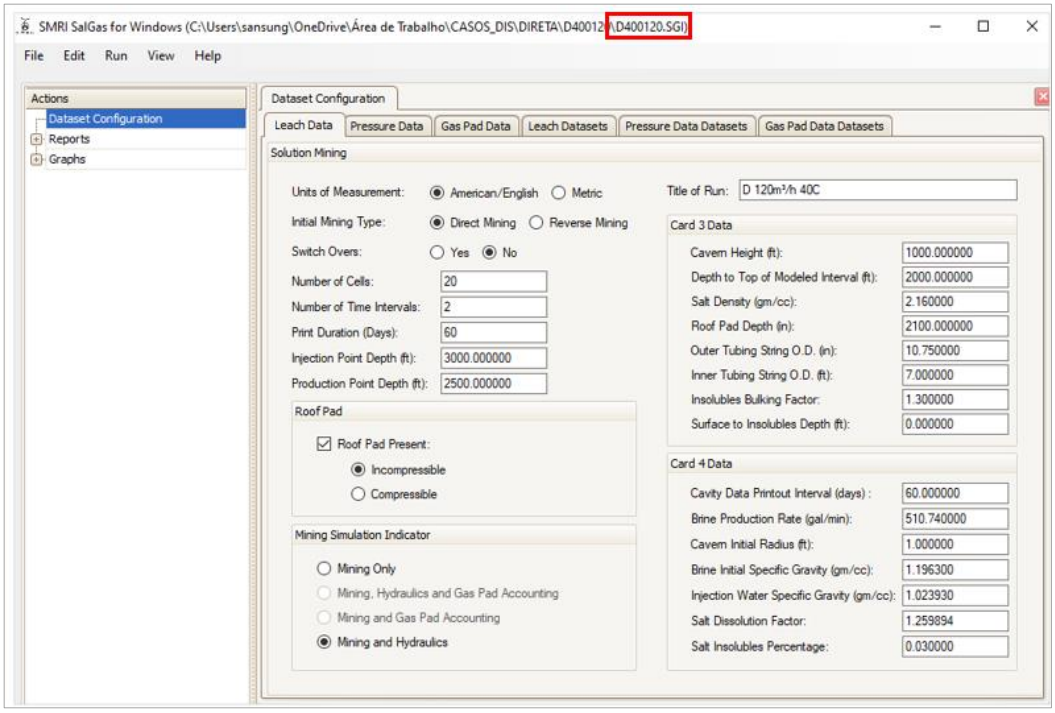

Source: The Author (2022).

Figure 9 – Running the case at SalGas: Given the start command

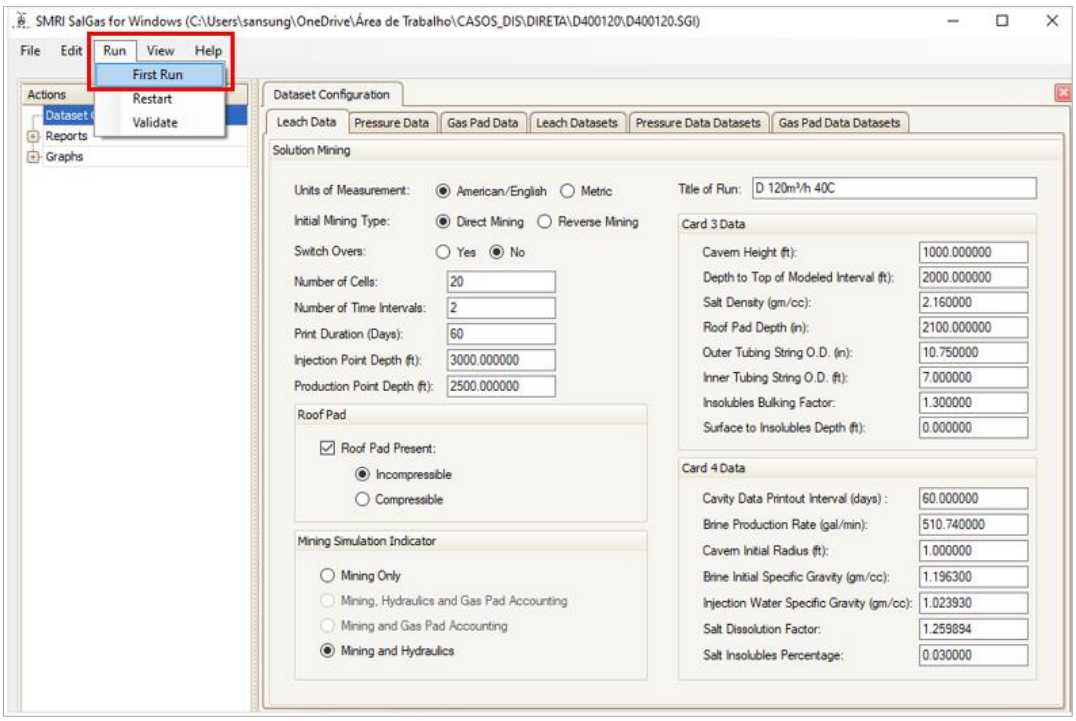

Source: The Author (2022).

Figure 10 – Running the case at SalGas: Wait for the simulation to complete

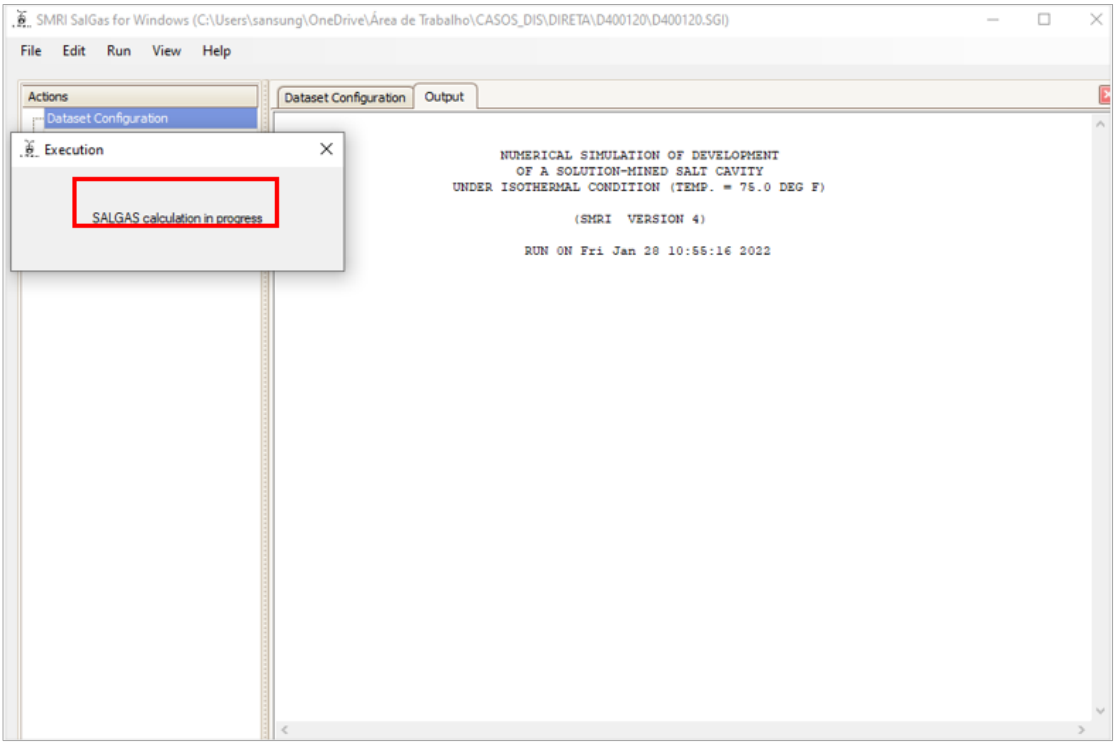

Source: The Author (2022).

Figure 11 – Running the case at SalGas: Check if it run until the end without error

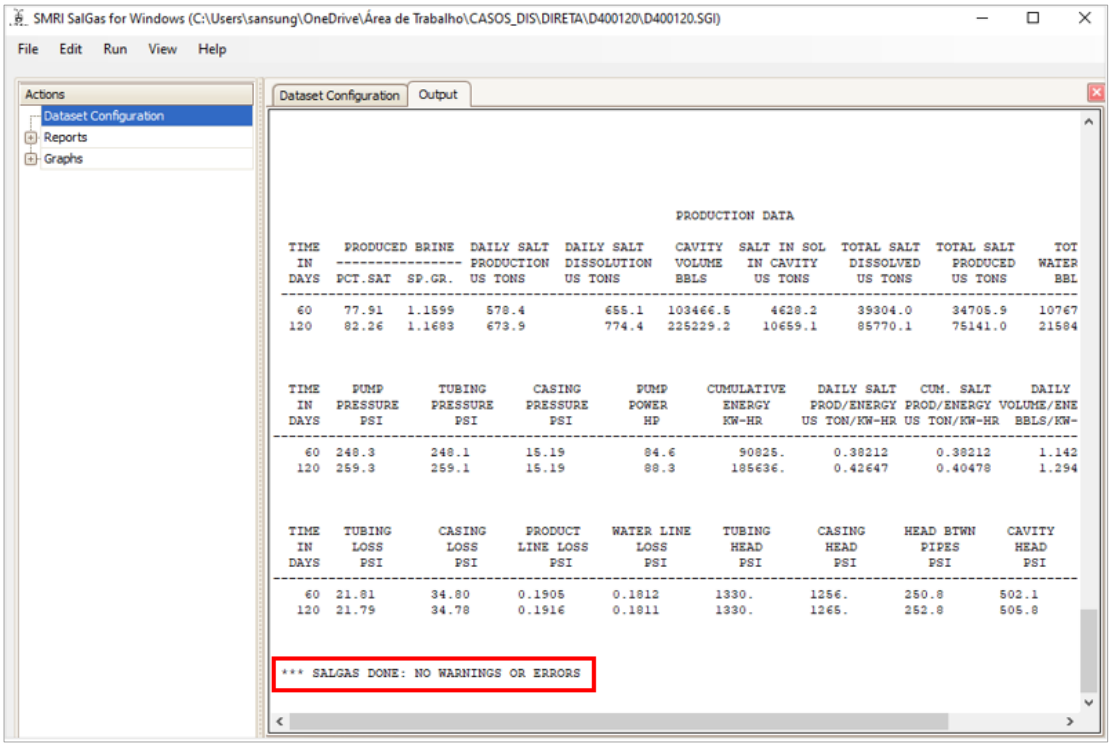

Source: The Author (2022).

5.2 INPUT DATA FOR THE PAST SOFTWARE

After running the cases in SALGAS, the production variables pump power, cumulative energy, tubing loss, brine produced and pump pressure in addition to the volume and radius of the cavern in the proposed final time (120 days) had their data selected together with the input variables injection temperature and brine production rate to be statistically analyzed by the PAST software, through the technique of principal component analysis (PCA).

The tables 7 and 8 below present these parameters, considering the two proposed scenarios.

Table 7 – Input parameters for the PAST software: Scenario D.

Injection Temperature (°C)	Injection Rate (m^3/h)	Radius (m)	Volume (m^3)	Pump Power (kW)	Cumulative Energy (J)	Tubing Loss (MPa)	Produced Brine (m^3)	Pump Pressure (MPa)	Injection Pressure (MPa)	Salt Dissolution Factor
40	120	7.7694	37213.41616	658.4531	6.6829E+11	0.1502	334211.3423	1.7878	9.0500	1.25989419
40	200	9.4031	57141.62737	1429.5069	1.45308E+12	0.3816	557057.8557	2.3318	9.1800	1.26016984
40	360	11.8049	92203.71572	4639.7454	4.73274E+12	1.1280	1002038.7796	4.2044	9.6700	1.26071911
40	400	12.2682	99816.80821	5941.7376	6.06455E+12	1.3755	1109596.3469	4.8381	9.8300	1.26099276
40	800	15.8313	166230.4175	34571.3977	3.56105E+13	4.9684	2230660.5850	14.1687	12.4200	1.26396075
40	1200	17.9192	212801.6161	103292.8726	1.08158E+14	10.4662	3329176.0150	28.5650	16.7400	1.26840665
60	120	8.3972	41667.42743	709.9064	7.21642E+11	0.1507	334211.3423	1.9154	9.0500	1.58798018
60	200	10.0614	64858.28877	1518.9909	1.54811E+12	0.3818	557057.8557	2.4656	9.1800	1.59017741
60	360	12.7224	106726.4532	4892.5377	4.96045E+12	1.1425	1002038.7796	4.3844	9.6700	1.59126914
60	400	13.2466	116042.2662	6068.5066	6.2317E+12	1.3617	1109596.3469	4.9463	9.8300	1.59235636
60	800	17.4315	201898.7646	35147.0781	3.62468E+13	4.9725	2230660.5850	14.3342	12.4200	1.60403307
60	1200	20.0497	265475.1015	104578.4594	1.09958E+14	10.4731	3329176.0150	28.7718	16.7400	1.62214403
80	120	8.7325	44843.31677	750.9199	7.6468E+11	0.1501	334211.3423	2.0209	9.0500	1.67090079
80	200	10.4760	70250.0149	1599.5265	1.62383E+12	0.3832	557057.8557	2.5786	9.1800	1.67697674
80	360	13.2801	116354.5469	4988.733	5.07783E+12	1.1321	1002038.7796	4.4685	9.6700	1.68871982
80	400	13.8440	126798.4618	6128.9083	6.34018E+12	1.3383	1109596.3469	5.0077	9.8300	1.69440201
80	800	18.4038	225757.1488	36343.9266	3.67627E+13	5.0421	2230660.5850	14.6307	12.4200	1.75029718
80	1200	21.4213	305255.9144	108662.6583	1.1227E+14	10.6800	3329176.0150	29.4406	16.7400	1.82428703

Source: The Author (2022).

Table 8 – Input parameters for the PAST software: Scenario R.

Injection Temperature (°C)	Injection Rate (m^3/h)	Radius (m)	Volume (m^3)	Pump Power (kW)	Cumulative Energy (J)	Tubing Loss (MPa)	Produced Brine (m^3)	Pump Pressure (MPa)	Injection Pressure (MPa)	Salt Dissolution Factor (DF)
40	120	9.7384	41584.35672	624.1509	6.38849E+11	0.1605	334211.3423	1.6885	7.5600	1.25822596
40	200	11.7653	64401.4905	1395.9504	1.42797E+12	0.4075	557057.8557	2.2698	7.7100	1.25850574
40	360	14.5786	104419.1241	4654.6594	4.77441E+12	1.1997	1002038.78	4.2106	8.2300	1.25878481
40	400	15.0967	113043.1148	5985.7339	6.12315E+12	1.4576	1109596.347	4.8629	8.4100	1.25906319
40	800	19.0378	189170.0651	34992.7182	3.67585E+13	5.2835	2230660.585	14.2997	11.2200	1.26235126
40	1200	21.3787	244061.1218	107118.3136	1.1174E+14	11.3074	3329176.015	29.5027	15.9000	1.26737505
60	120	10.4638	45842.4658	659.9445	6.78539E+11	0.1609	334211.3423	1.7802	7.5600	1.58127404
60	200	12.7467	72203.79183	1457.0978	1.49936E+12	0.4087	557057.8557	2.3670	7.7100	1.58240401
60	360	15.9258	119336.2686	4803.7994	4.92558E+12	1.2045	1002038.78	4.3265	8.2300	1.58464903
60	400	16.5384	129867.4276	6131.8911	6.29215E+12	1.4638	1109596.347	4.9718	8.4100	1.58576420
60	800	21.1988	225099.0809	35408.0731	3.69047E+13	5.3159	2230660.585	14.5204	11.2200	1.59878792
60	1200	24.2286	300251.0434	110101.8593	1.13889E+14	11.3901	3329176.015	29.9646	15.9000	1.61821655
80	120	10.8692	48891.77127	693.501	7.13102E+11	0.1609	334211.3423	1.8643	7.5600	1.63097469
80	200	13.2862	77437.07788	1517.4995	1.55969E+12	0.4087	557057.8557	2.4518	7.7100	1.63810134
80	360	16.6634	128735.2716	4864.9468	5.02142E+12	1.2045	1002038.78	4.3906	8.2300	1.65174855
80	400	17.3401	140390.4591	6262.3886	6.42679E+12	1.4638	1109596.347	5.0566	8.4100	1.65829672
80	800	22.4516	248085.5009	35762.2806	3.71783E+13	5.3221	2230660.585	14.6031	11.2200	1.72622905
80	1200	26.0634	339761.6182	110544.8051	1.14688E+14	11.4108	3329176.015	30.0060	15.9000	1.80920606

Source: The Author (2022).

The sequence of figures 12 to 17 illustrate how the PAST software performs the multivariate analysis, from the selection of data from Excel to the generation of graphs and tables.

Figure 12 – Input data for the PAST: Select data in EXCEL

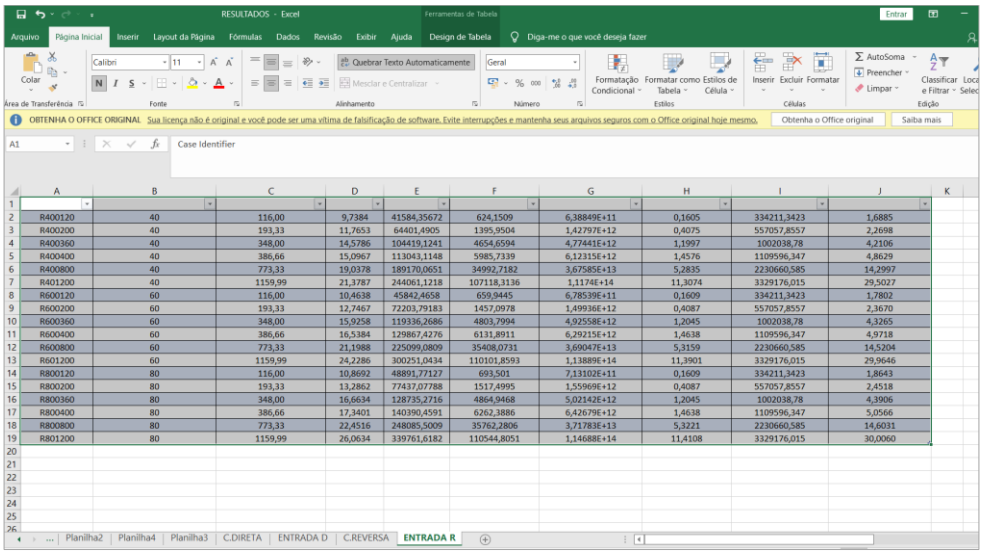

	A	B	C	D	E	F	G	H	I	J
1										
2	R400120	40	116,00	9,7384	41584,35672	624,1509	6,38849E+11	0,1605	334211,3423	1,6885
3	R400200	40	193,33	11,7653	64401,4905	1395,9504	1,42797E+12	0,4075	557057,8557	2,2698
4	R400360	40	348,00	14,5786	104419,1241	4654,6594	4,77441E+12	1,1997	1002038,78	4,2106
5	R400400	40	386,66	15,0967	113043,1148	5985,7339	6,12315E+12	1,4576	1109596,347	4,8629
6	R400800	40	773,33	19,0378	189170,0651	34992,7182	3,67585E+13	5,2835	2230660,585	14,2997
7	R401200	40	1159,99	21,3787	244061,1218	107118,3136	1,1174E+14	11,3074	3329176,015	29,5027
8	R600120	60	116,00	10,4638	45842,4658	659,9445	6,78539E+11	0,1609	334211,3423	1,7802
9	R600200	60	193,33	12,7467	72203,79183	1457,0978	1,49936E+12	0,4087	557057,8557	2,3670
10	R600360	60	348,00	15,9258	119336,2686	4803,7994	4,92558E+12	1,2045	1002038,78	4,3265
11	R600400	60	386,66	16,5384	129867,4276	6131,8911	6,29215E+12	1,4638	1109596,347	4,9718
12	R600800	60	773,33	21,1988	225099,0809	35408,0731	3,69047E+13	5,3159	2230660,585	14,5204
13	R601200	60	1159,99	24,2286	300251,0434	110101,8593	1,13889E+14	11,3901	3329176,015	29,9646
14	R800120	80	116,00	10,8692	48891,77127	693,501	7,13102E+11	0,1609	334211,3423	1,8643
15	R800200	80	193,33	13,2862	77437,07788	1517,4995	1,55969E+12	0,4087	557057,8557	2,4518
16	R800360	80	348,00	16,6634	128735,2716	4864,9468	5,02142E+12	1,2045	1002038,78	4,3906
17	R800400	80	386,66	17,3401	140390,4591	6262,3886	6,42679E+12	1,4638	1109596,347	5,0566
18	R800800	80	773,33	22,4516	248085,5009	35762,2806	3,71783E+13	5,3221	2230660,585	14,6031
19	R801200	80	1159,99	26,0634	339761,6182	110544,8051	1,14688E+14	11,4108	3329176,015	30,0060
20										
21										
22										
23										
24										
25										
26										

Source: The Autor (2022).

Figure 13 – Input data for the PAST: Open the PAST and select “Row attributes” and “Column attributes”

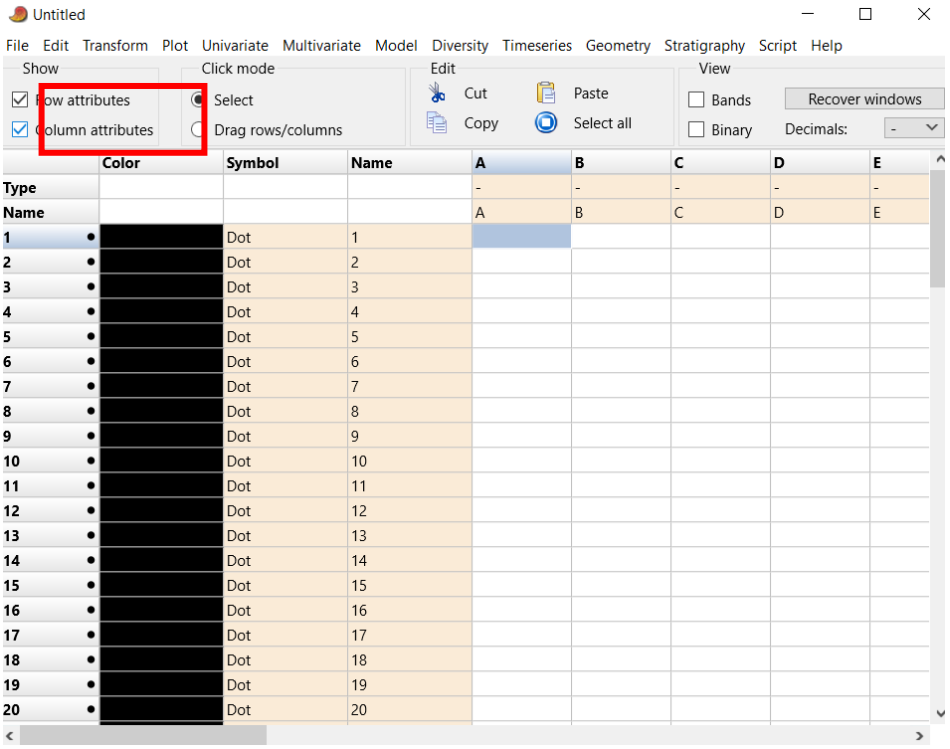

	Color	Symbol	Name	A	B	C	D	E
Type				-	-	-	-	-
Name				A	B	C	D	E
1		Dot	1					
2		Dot	2					
3		Dot	3					
4		Dot	4					
5		Dot	5					
6		Dot	6					
7		Dot	7					
8		Dot	8					
9		Dot	9					
10		Dot	10					
11		Dot	11					
12		Dot	12					
13		Dot	13					
14		Dot	14					
15		Dot	15					
16		Dot	16					
17		Dot	17					
18		Dot	18					
19		Dot	19					
20		Dot	20					

Source: The Autor (2022).

Figure 14 – Input data for the PAST: Paste EXCEL data in highlighted space

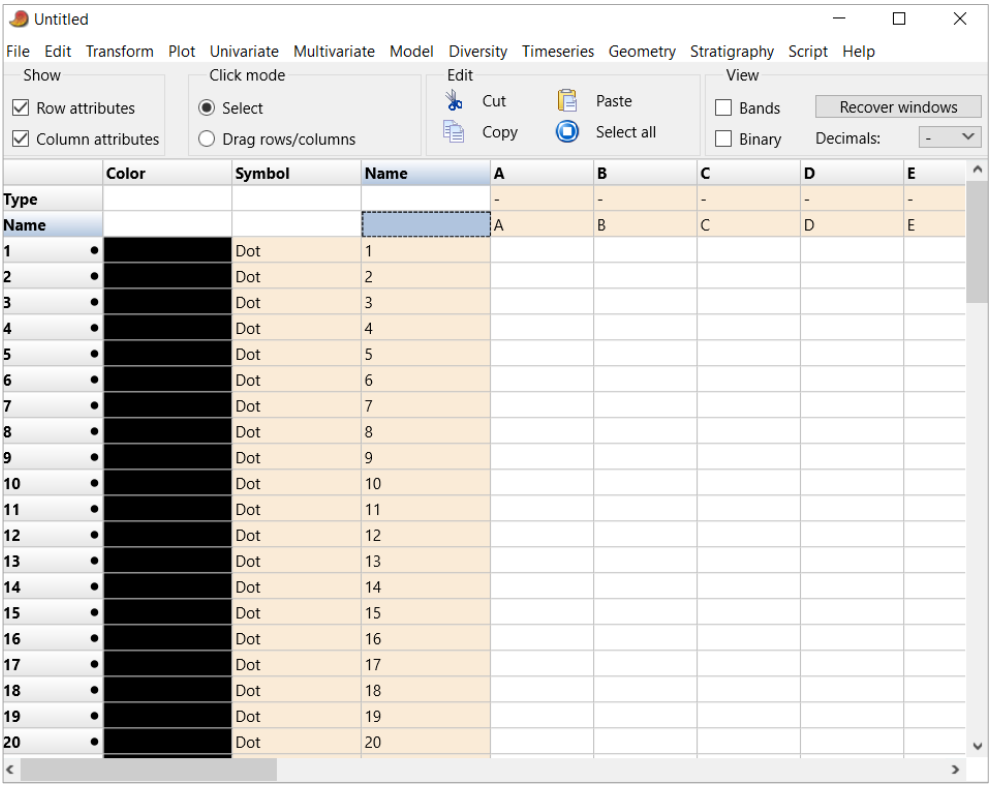

	Color	Symbol	Name	A	B	C	D	E
Type				-	-	-	-	-
Name				A	B	C	D	E
1		Dot	1					
2		Dot	2					
3		Dot	3					
4		Dot	4					
5		Dot	5					
6		Dot	6					
7		Dot	7					
8		Dot	8					
9		Dot	9					
10		Dot	10					
11		Dot	11					
12		Dot	12					
13		Dot	13					
14		Dot	14					
15		Dot	15					
16		Dot	16					
17		Dot	17					
18		Dot	18					
19		Dot	19					
20		Dot	20					

Source: The Autor (2022).

Figure 15 – Input data for the PAST: Data are selected

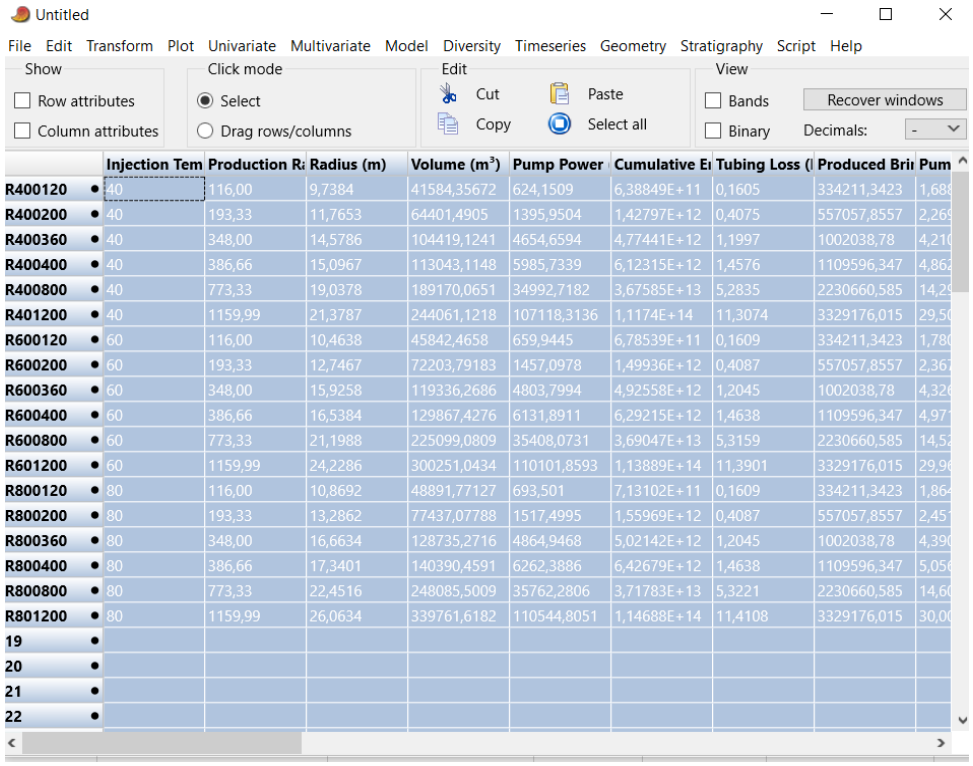

	Injection Tem	Production Ra	Radius (m)	Volume (m³)	Pump Power	Cumulative E	Tubing Loss (I	Produced Bri	Pum
R400120	40	116,00	9,7384	41584,35672	624,1509	6,38849E+11	0,1605	334211,3423	1,68
R400200	40	193,33	11,7653	64401,4905	1395,9504	1,42797E+12	0,4075	557057,8557	2,26
R400360	40	348,00	14,5786	104419,1241	4654,6594	4,77441E+12	1,1997	1002038,78	4,21
R400400	40	386,66	15,0967	113043,1148	5985,7339	6,12315E+12	1,4576	1109596,347	4,86
R400800	40	773,33	19,0378	189170,0651	34992,7182	3,67585E+13	5,2835	2230660,585	14,2
R401200	40	1159,99	21,3787	244061,1218	107118,3136	1,1174E+14	11,3074	3329176,015	29,5
R600120	60	116,00	10,4638	45842,4658	659,9445	6,78539E+11	0,1609	334211,3423	1,78
R600200	60	193,33	12,7467	72203,79183	1457,0978	1,49936E+12	0,4087	557057,8557	2,36
R600360	60	348,00	15,9258	119336,2686	4803,7994	4,92558E+12	1,2045	1002038,78	4,32
R600400	60	386,66	16,5384	129867,4276	6131,8911	6,29215E+12	1,4638	1109596,347	4,97
R600800	60	773,33	21,1988	225099,0809	35408,0731	3,69047E+13	5,3159	2230660,585	14,5
R601200	60	1159,99	24,2286	300251,0434	110101,8593	1,13889E+14	11,3901	3329176,015	29,9
R800120	80	116,00	10,8692	48891,77127	693,501	7,13102E+11	0,1609	334211,3423	1,86
R800200	80	193,33	13,2862	77437,07788	1517,4995	1,55969E+12	0,4087	557057,8557	2,45
R800360	80	348,00	16,6634	128735,2716	4864,9468	5,02142E+12	1,2045	1002038,78	4,39
R800400	80	386,66	17,3401	140390,4591	6262,3886	6,42679E+12	1,4638	1109596,347	5,05
R800800	80	773,33	22,4516	248085,5009	35762,2806	3,71783E+13	5,3221	2230660,585	14,6
R801200	80	1159,99	26,0634	339761,6182	110544,8051	1,14688E+14	11,4108	3329176,015	30,0
19									
20									
21									
22									

Source: The Autor (2022).

Figure 16 – Input data for the PAST: Select the option “multivariate” > “ordination” > “PCA”

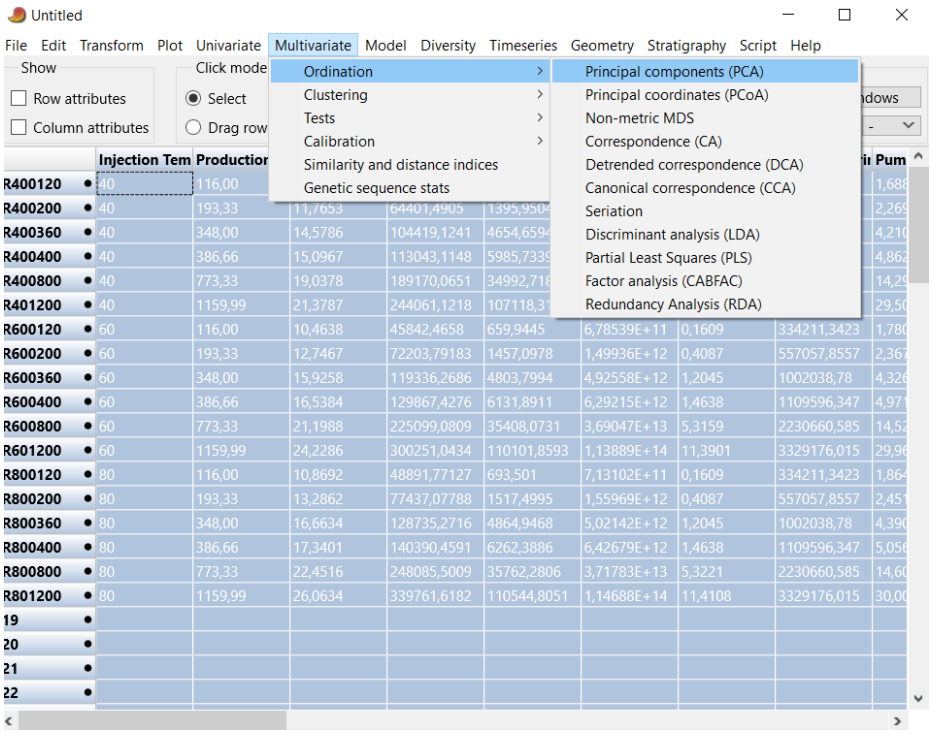

Source: The Autor (2022).

Figure 17 – Input data for the PAST: Select the option “correlation” then the command “recompute”

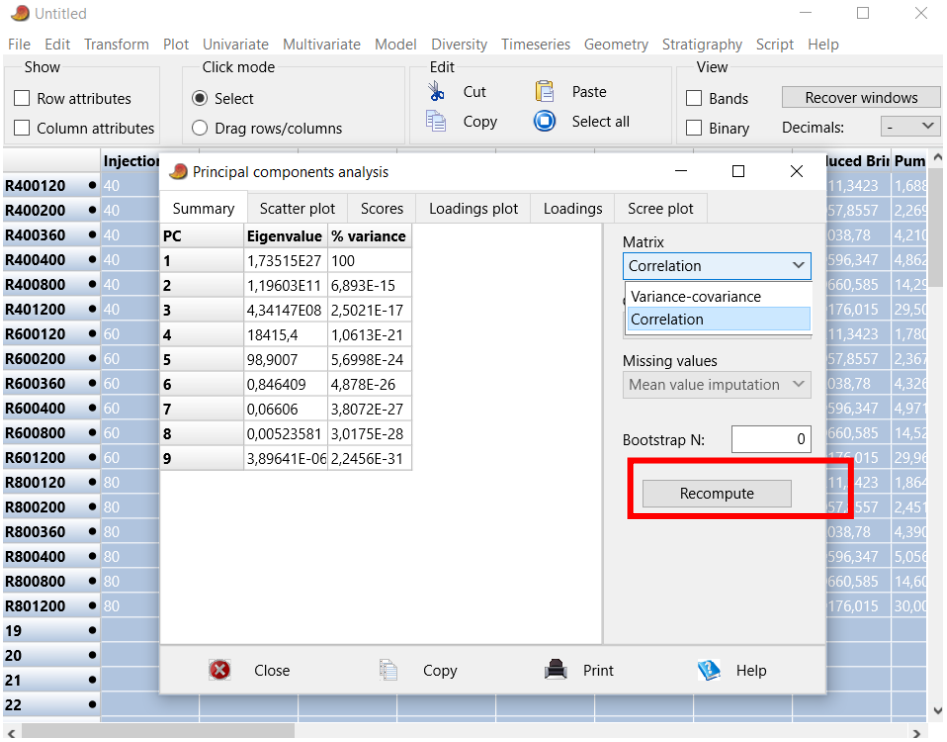

Source: The Autor (2022).

6 RESULTS AND DISCUSSIONS

This chapter presents the main simulations obtained with the SALGAS software and the statistical analysis of the data with the PAST software.

6.1 RESULTS WITH SALGAS

Based on the simulations performed in the SALGAS software, it was possible to obtain response surfaces for both the D and R scenarios. The behavior of the cavern was analyzed considering the variation of the injection temperature and the brine production rate along of time of 120 days.

Figures 18 to 25 bring the main simulations for scenario D.

The comparison between the final contours of the cavern for the time of 120 days considering each case analyzed was presented in figures 19 to 21, where it was possible to verify the geometry and the value of the radius reached. For the same temperature, the higher the production rate, the greater the radius of the cave. The maximum value reached for the time of 120 days was of approximately 22 m of radius for the temperature of 80ºC and injection rate of 1200 m³/h. Analyzing the same rate value, the cavern radius increases with increasing temperature, but this seems to have less influence on the final diameter obtained than the rate.

Figure 18 – Comparison of final cavern contours: T = 40°C

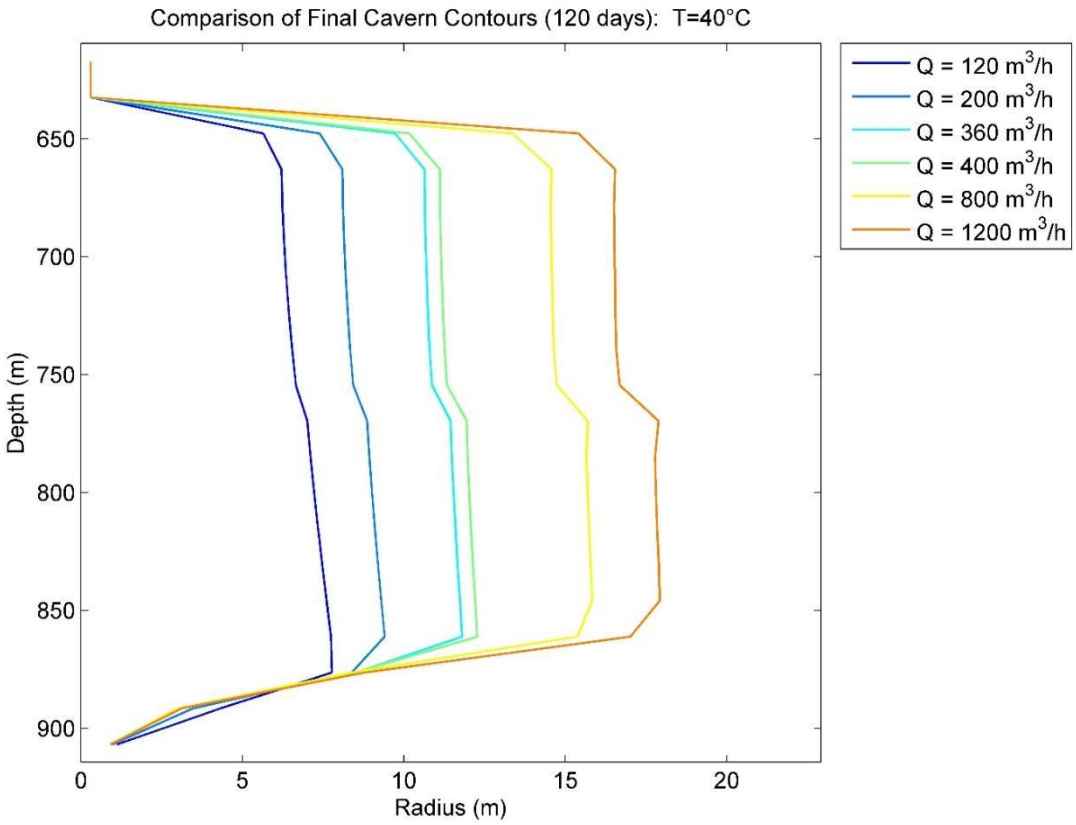

Source: The Autor (2022).

Figure 19 – Comparison of final cavern contours: T = 60°C

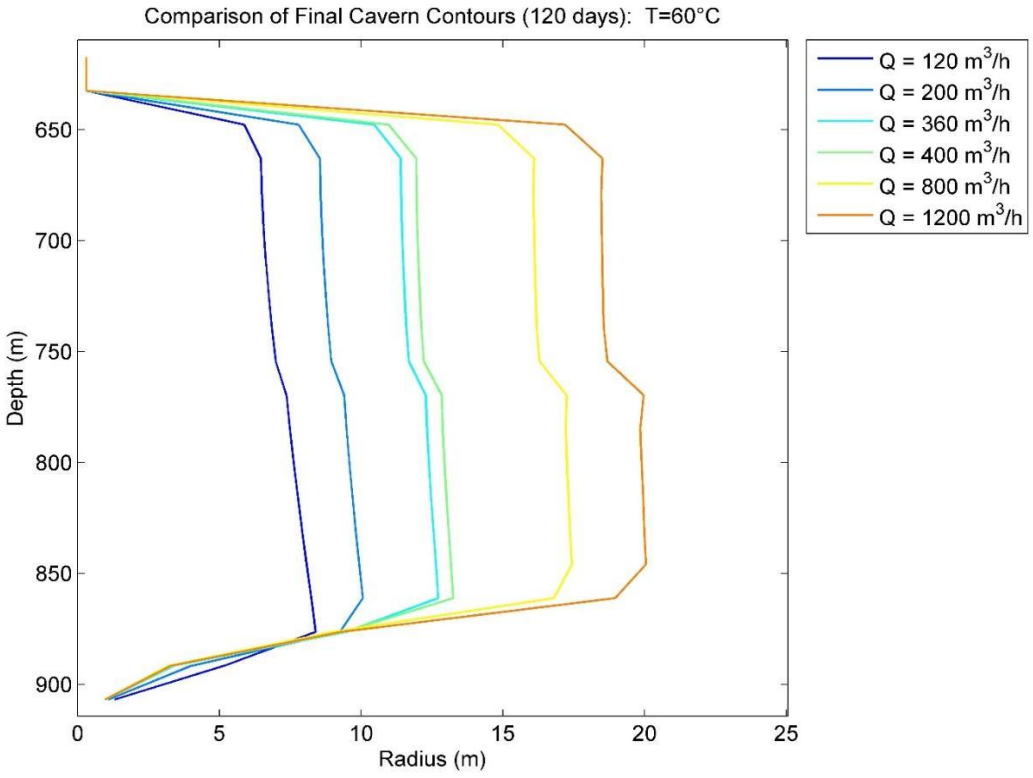

Source: The Autor (2022).

Figure 20 – Comparison of final cavern contours: T = 80°C

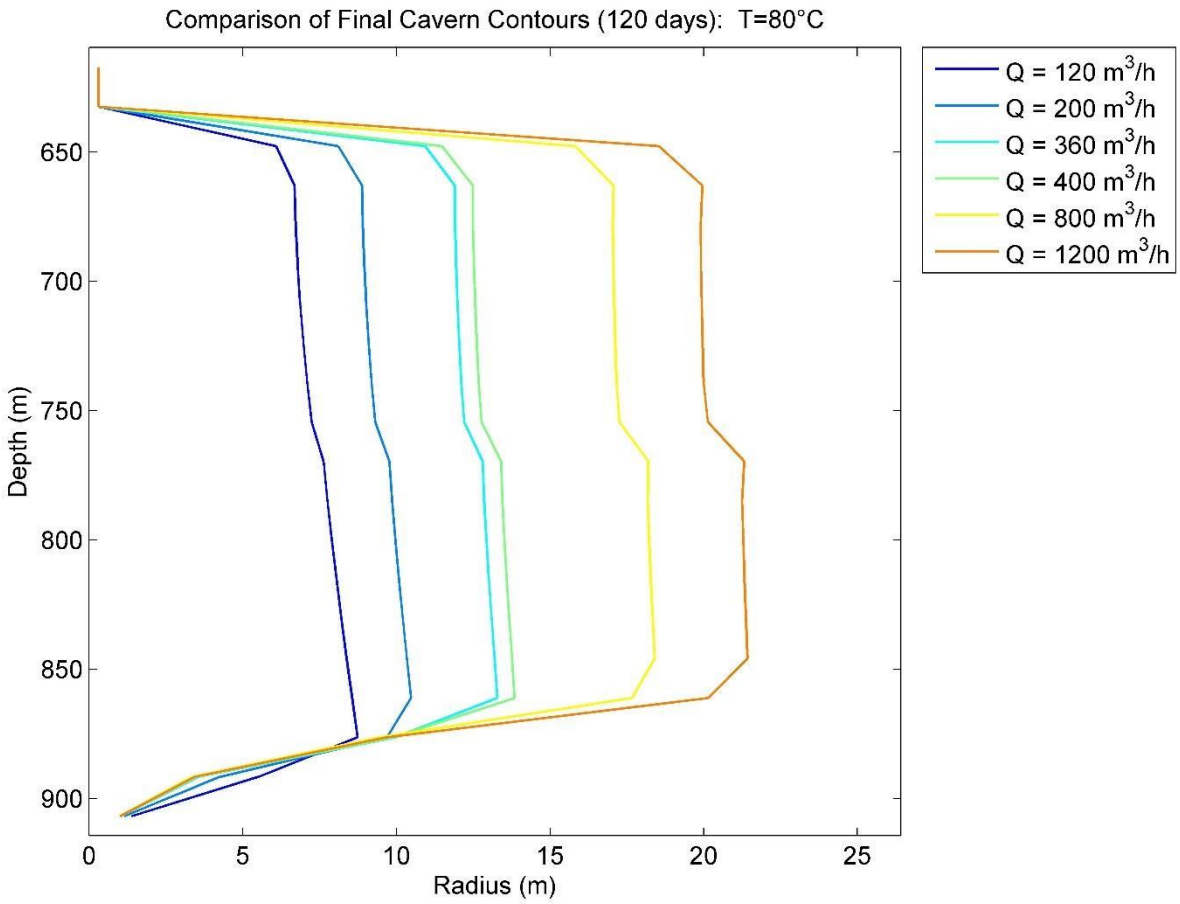

Source: The Autor (2022).

The comparison of the final geometry obtained in all analyzed cases, for different flows and temperatures, is illustrated in figure 21. The influence of temperature on the cavern geometry can be better observed. The radius shows a variation along the depth, decreasing as it moves away from the injection point, this behavior being more expressive with the increase in temperature.

Figure 21 – Comparison of final cavern contours: all simulations

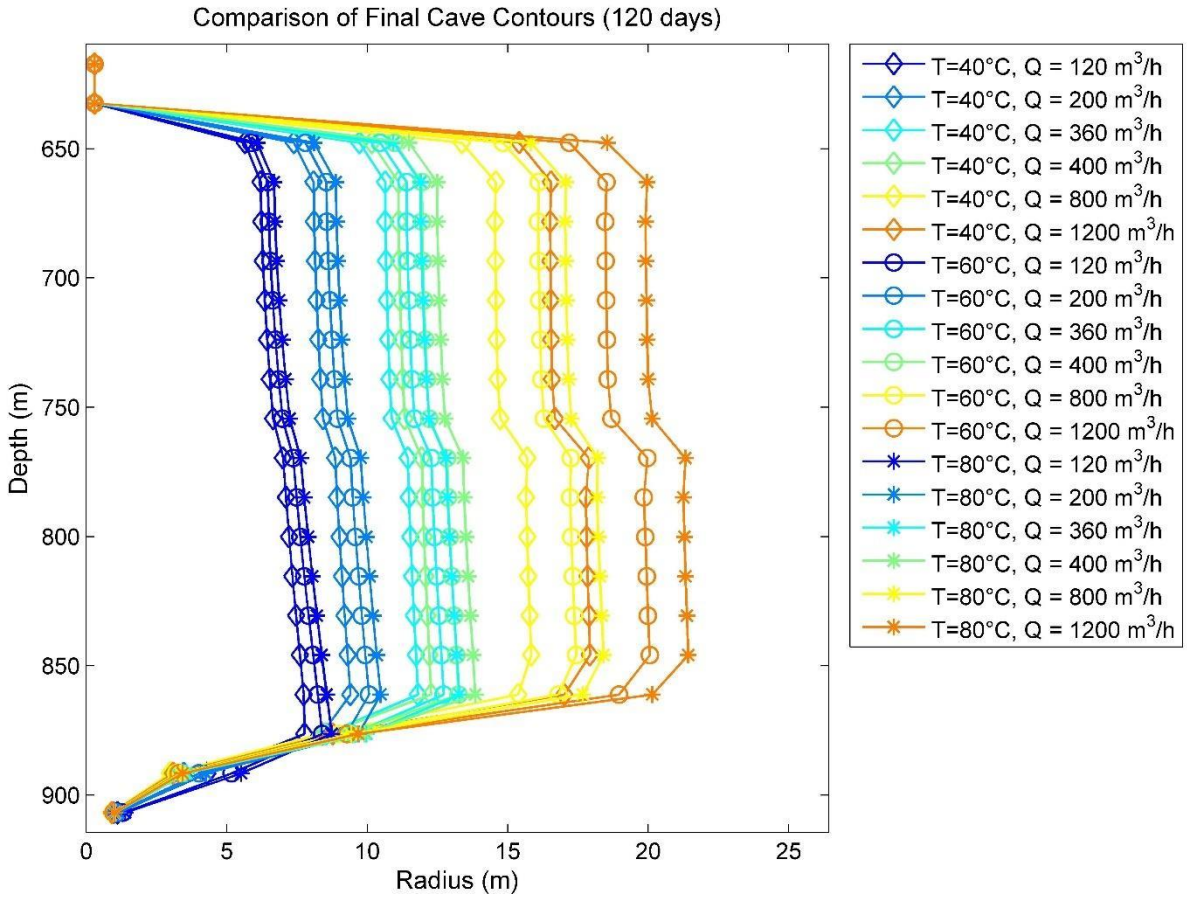

Source: The Autor (2022).

In addition to the cavern geometry, the evolution of its volume was evaluated, as indicated in the sequence of figures below (Figure 22 to Figure 24), where the results of all rates for each temperature are presented. For the same temperature, the volume grows faster for higher rates. Figure 25 shows the evolution of the cavern volume for all cases analyzed (all rates and temperatures). Analyzing the influence of temperature, it is observed that for the same rate, the higher the temperature, the greater the volume of the cavern.

Figure 22 – Cavern Volume Evolution: T = 40°C

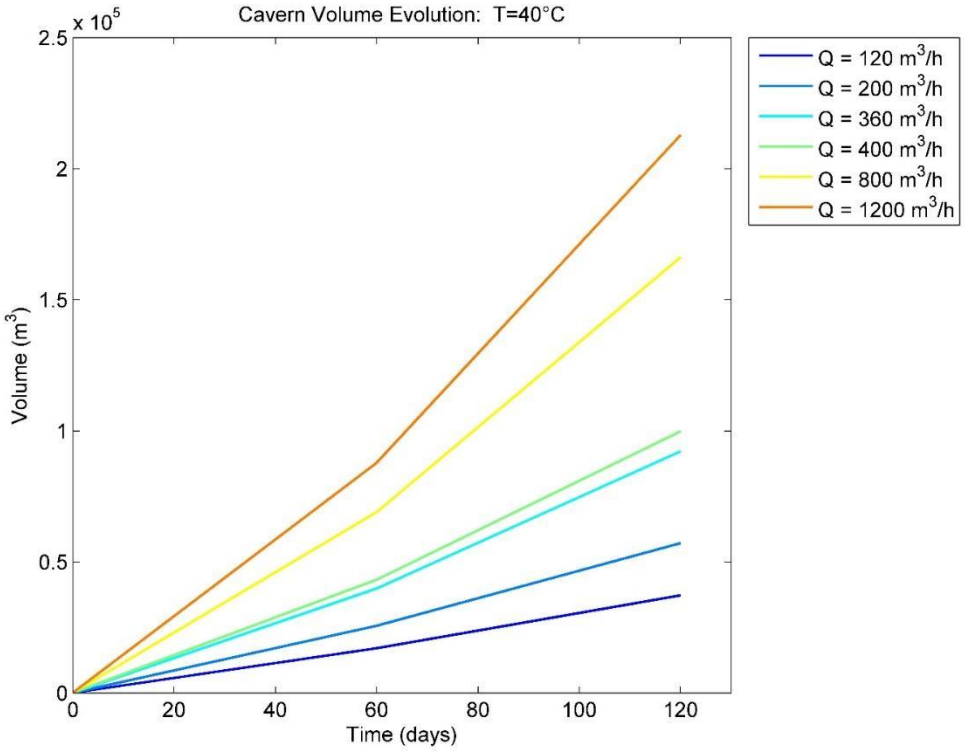

Source: The Autor (2022).

Figure 23 – Cavern Volume Evolution: T = 60°C

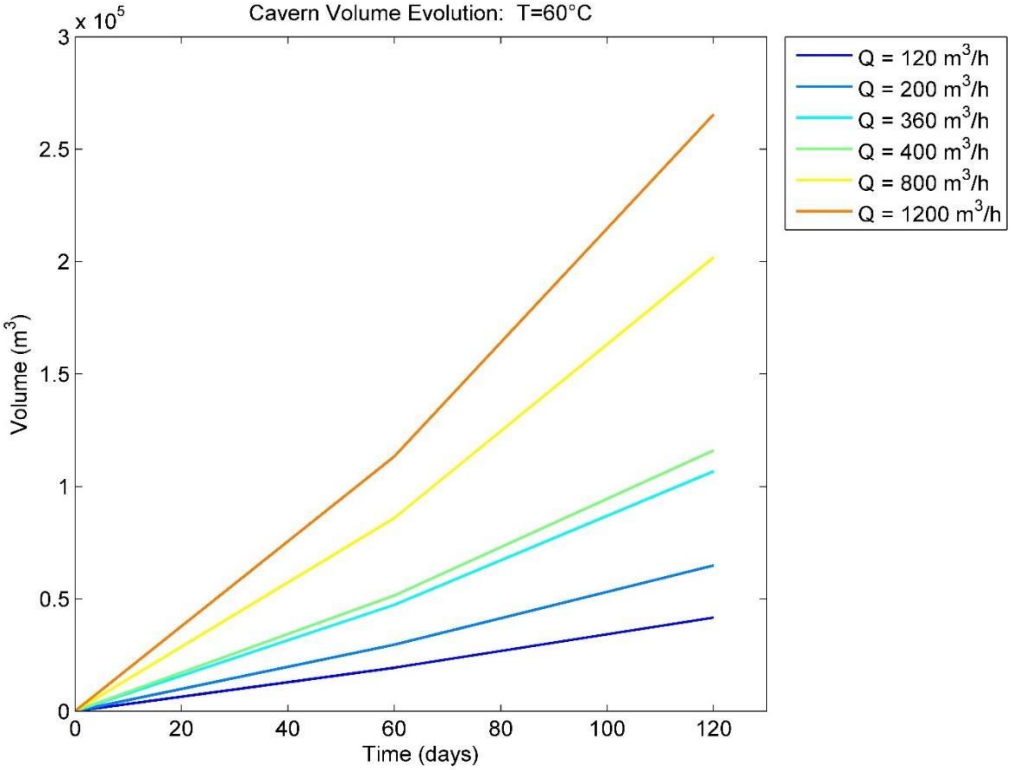

Source: The Autor (2022).

Figure 24 – Cavern Volume Evolution: T = 80°C

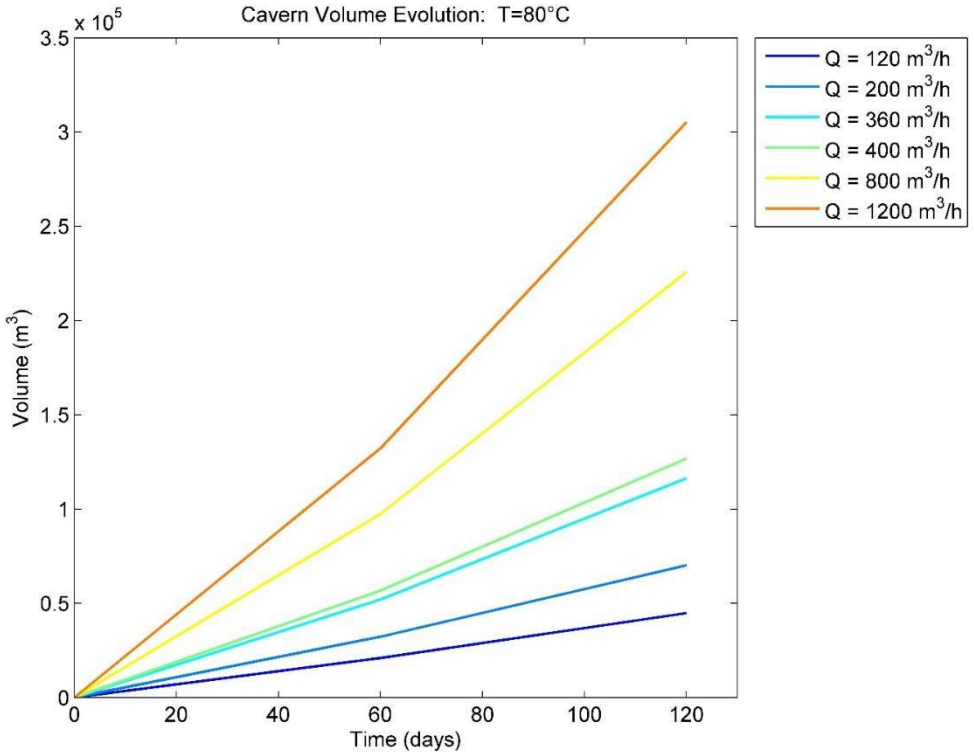

Source: The Autor (2022).

Figure 25 – Comparison of Cavern Volume Evolution: all simulations

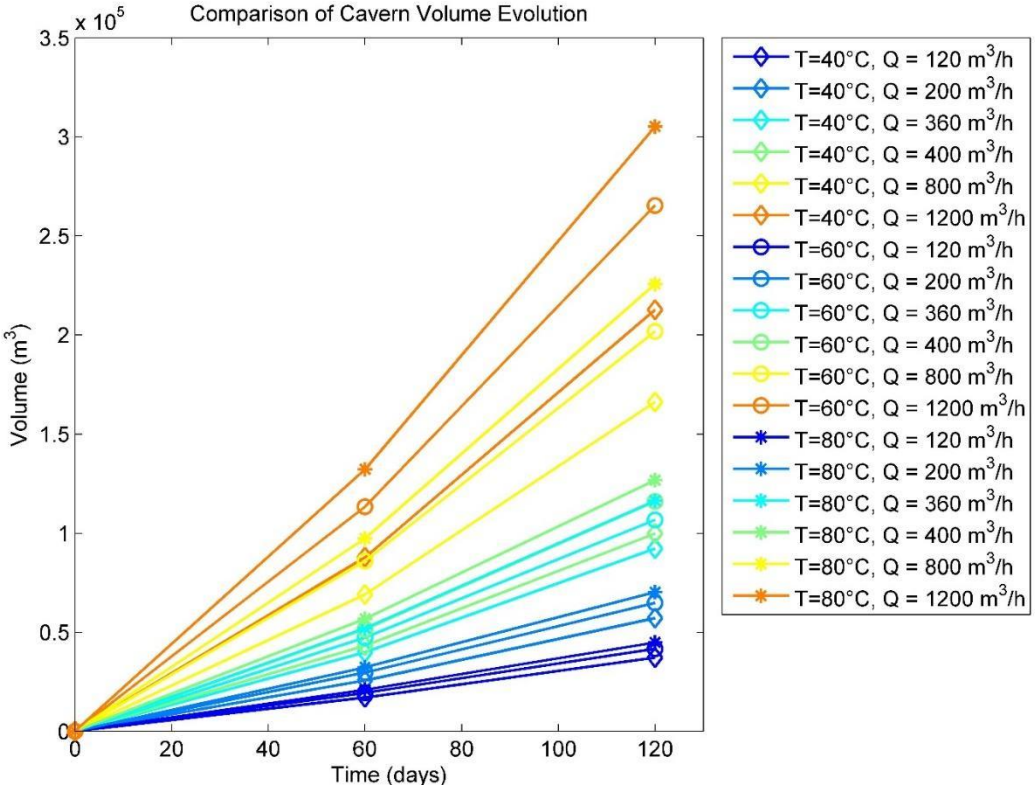

Source: The Autor (2022).

Figures 26 to 33 bring the main simulations for scenario R.

The comparison between the final contours of the cavern for the time of 120 days considering each case analyzed was presented in figures 26 to 28, where it was possible to verify the geometry and the value of the radius reached. Similar to what happens in scenario D, for the same temperature, the higher the production rate, the greater the radius of the cavern. The maximum value reached for the time of 120 days was approximately 26 m of radius for the temperature of 80ºC and injection rate of 1200 m³/h. Analyzing the same rate value, the cavern radius increases with increasing temperature, but this seems to have less influence on the final diameter obtained than the rate.

Figure 26 – Comparison of final cavern contours: T = 40°C

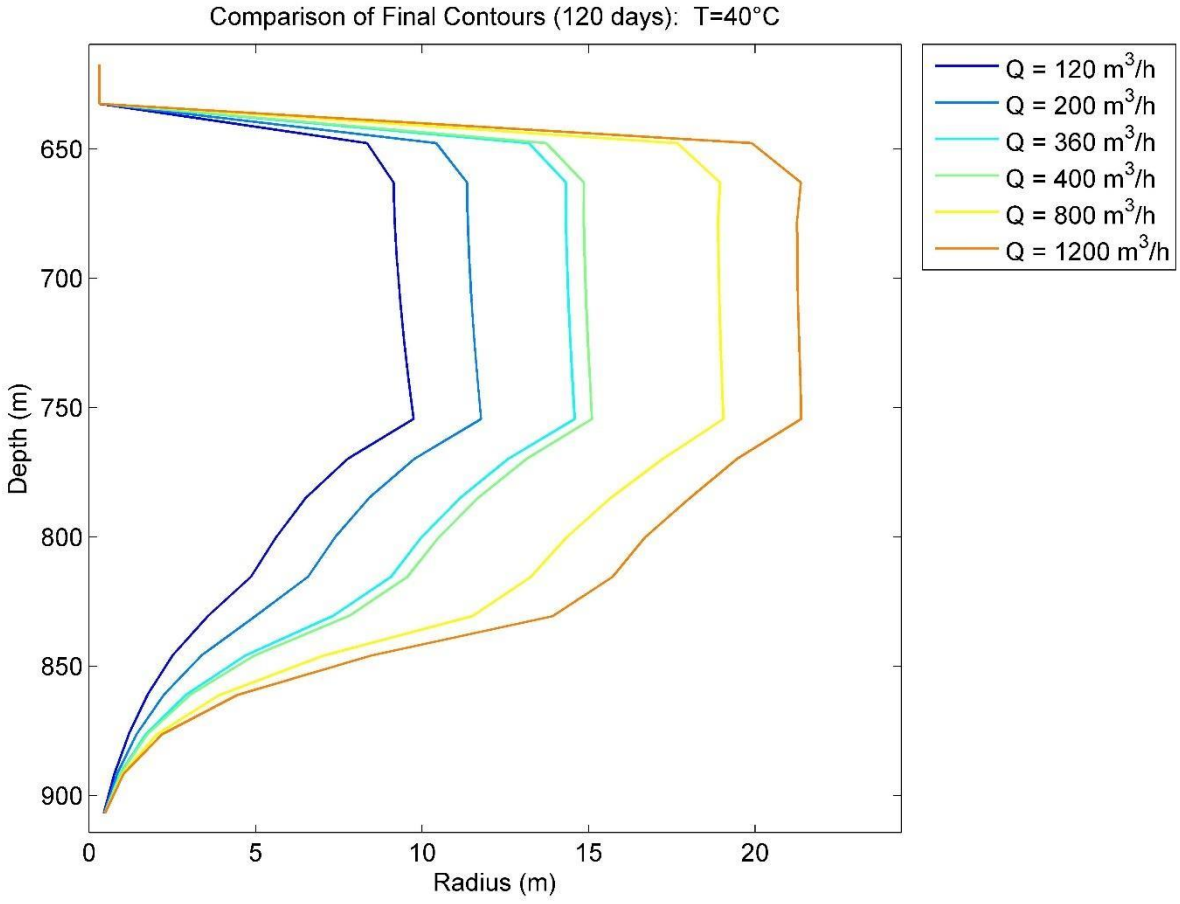

Source: The Autor (2022).

Figure 27 – Comparison of final cavern contours: T = 60°C

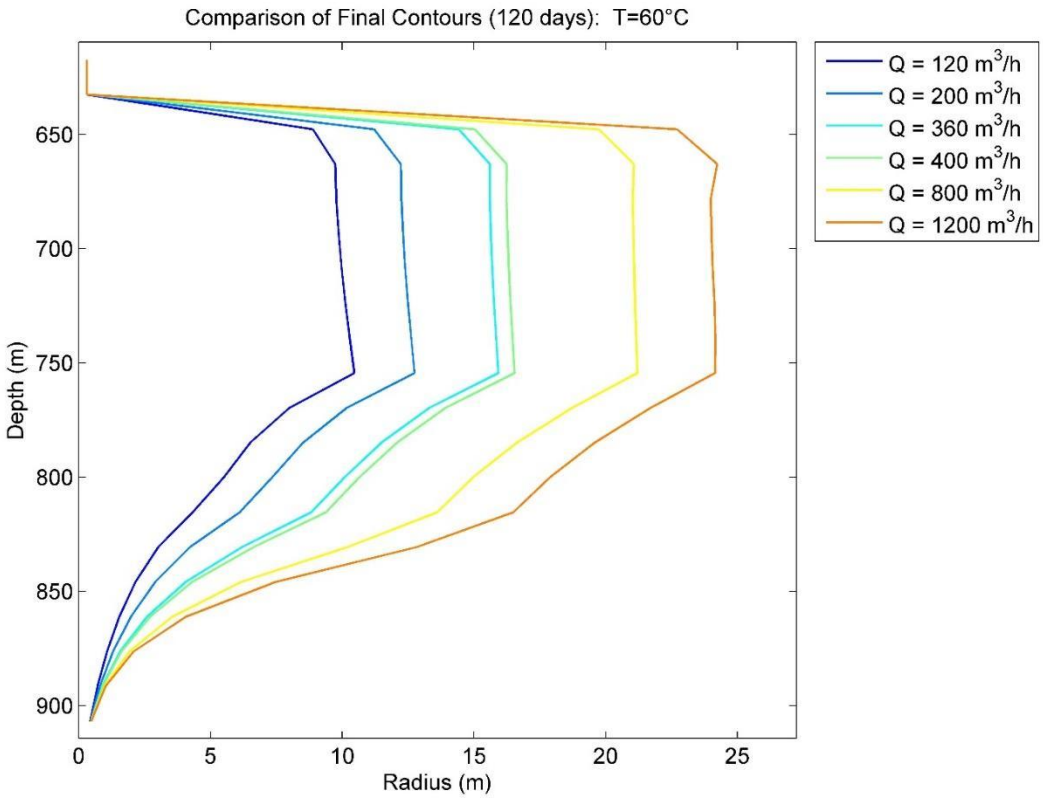

Source: The Autor (2022).

Figure 28 – Comparison of final cavern contours: T = 80°C

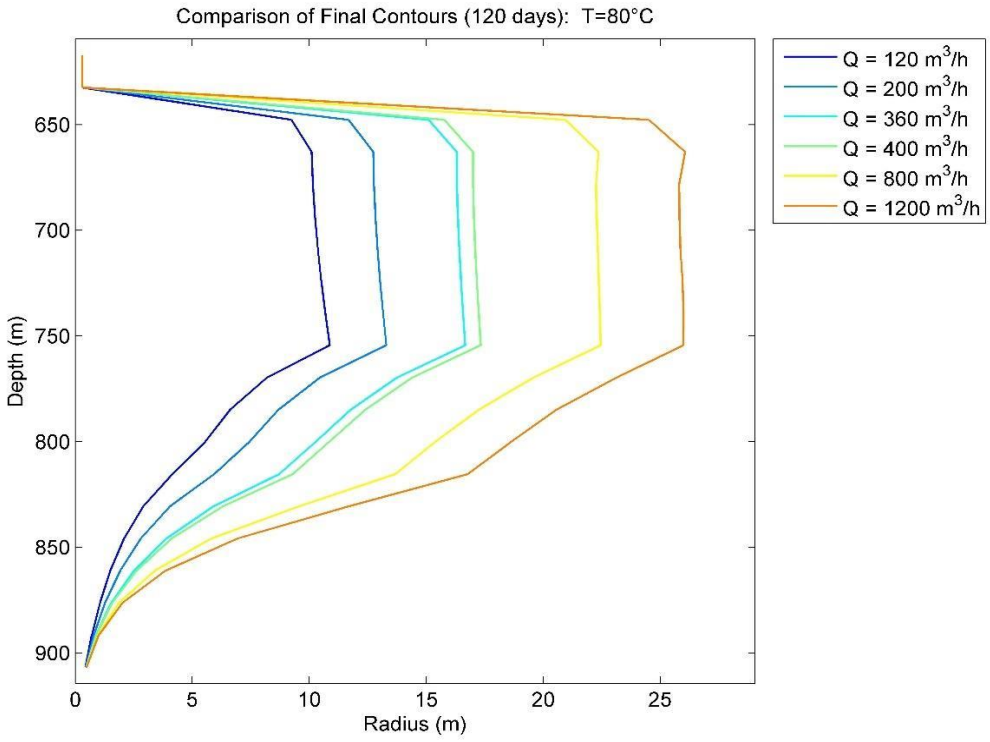

Source: The Autor (2022).

The comparison of the final geometry obtained in all cases analyzed, for different flows and temperatures, is illustrated in Figure 29.

Figure 29 – Comparison of final cavern contours: all simulations

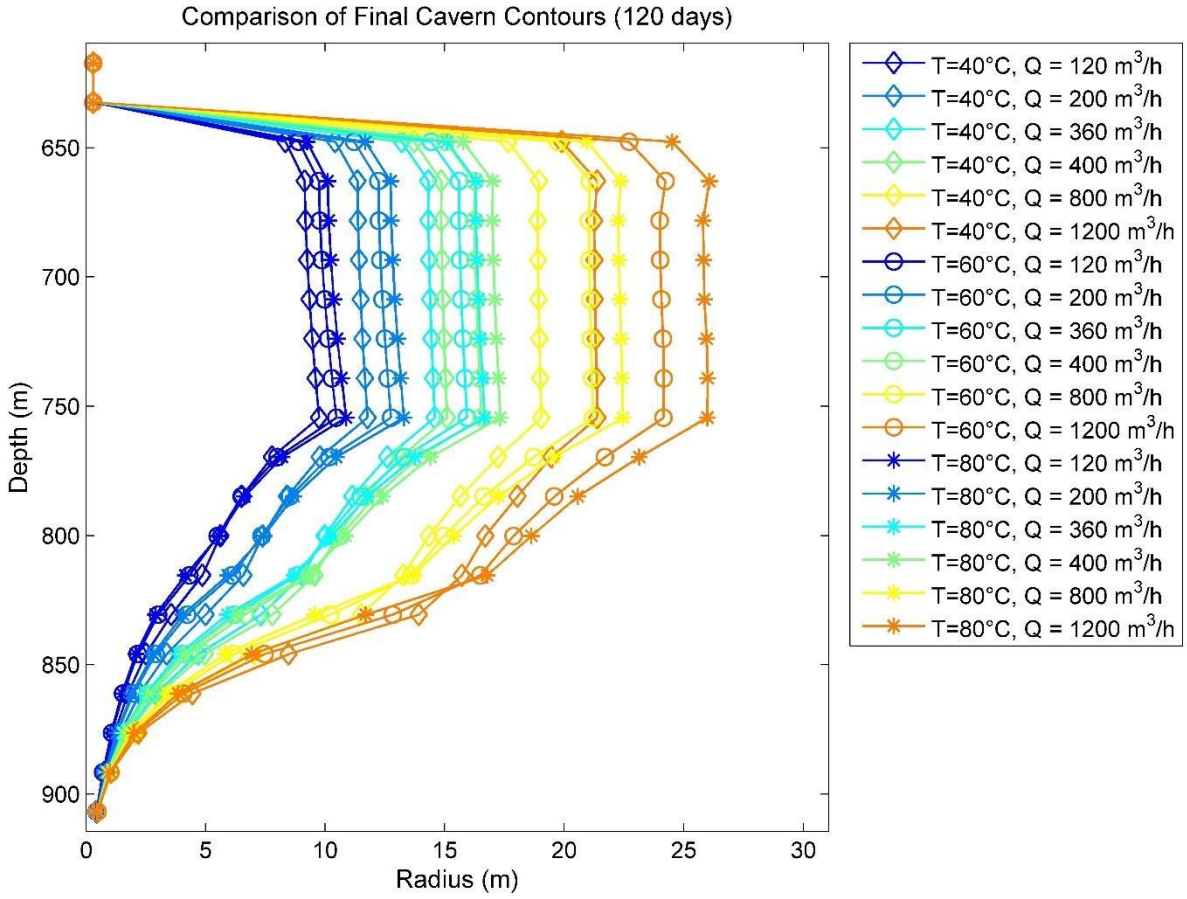

Source: The Autor (2022).

In addition to the cavern geometry, the evolution of its volume was evaluated, as indicated in the sequence of figures below (Figure 30 to Figure 32), where the results of all rates for each temperature are presented. Simulate what happens in scenario D, for the same temperature, the volume grows faster for higher rates. Figure 33 shows the evolution of the cavern volume for all cases analyzed (all rates and temperatures). Analyzing the influence of temperature, it is observed that for the same rate, the higher the temperature, the greater the volume of the cavern.

Figure 30 – Cavern Volume Evolution: T = 40°C

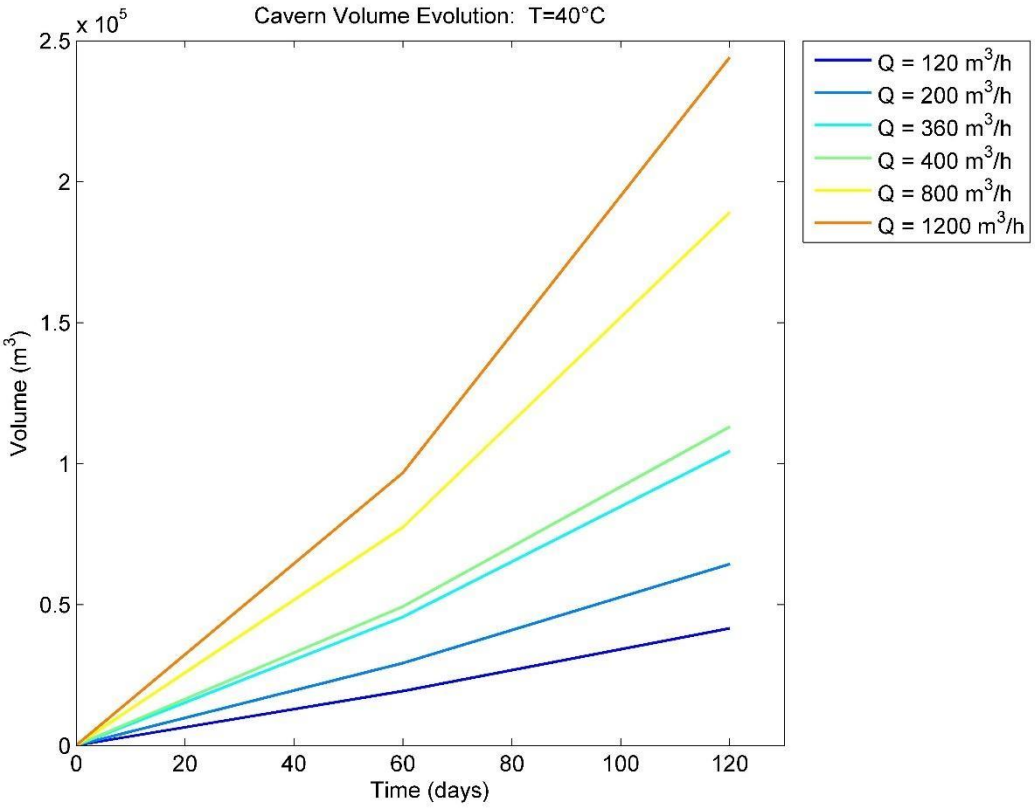

Source: The Autor (2022).

Figure 31 – Cavern Volume Evolution: T = 60°C

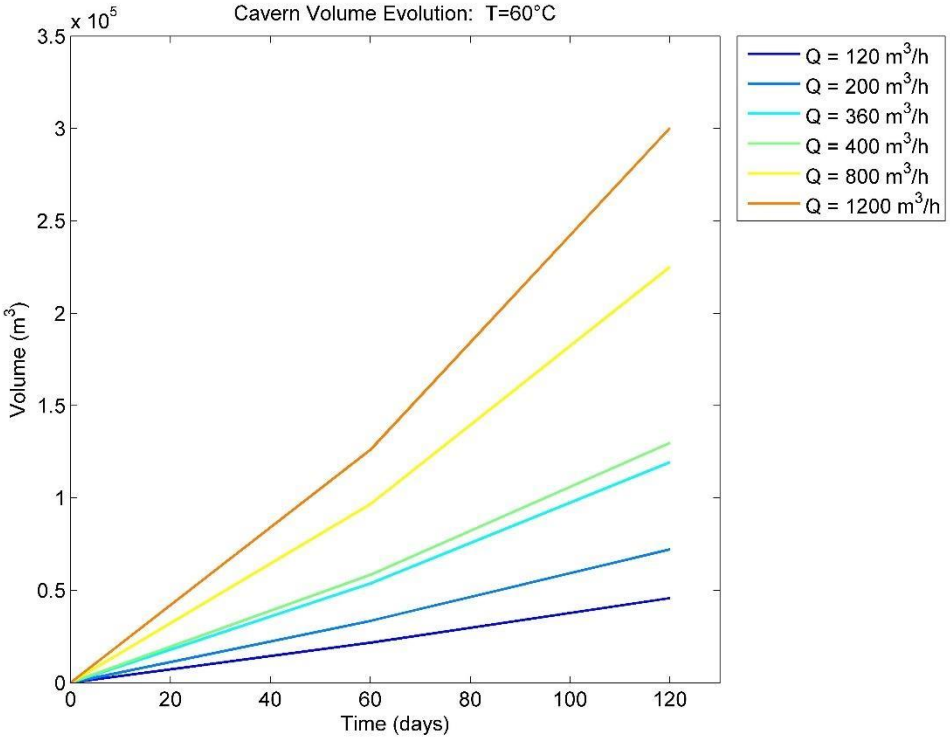

Source: The Autor (2022).

Figure 32 – Cave Volume Evolution: T = 80°C

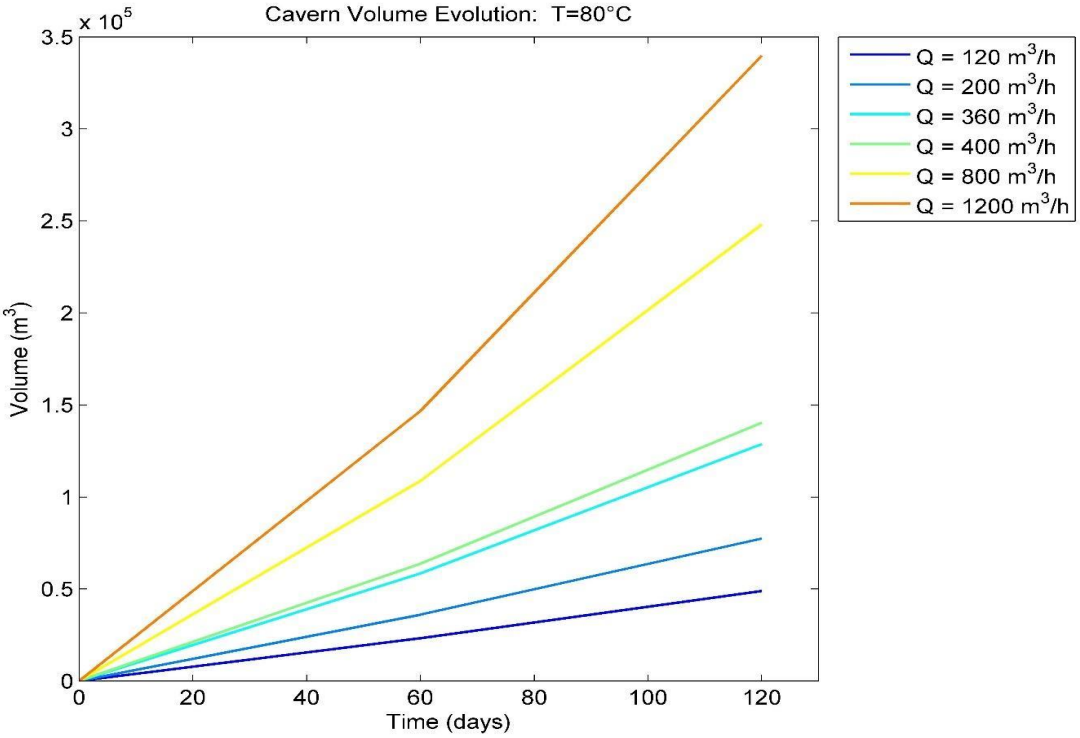

Source: The Autor (2022).

Figure 33 – Comparison of Cave Volume Evolution: all simulations

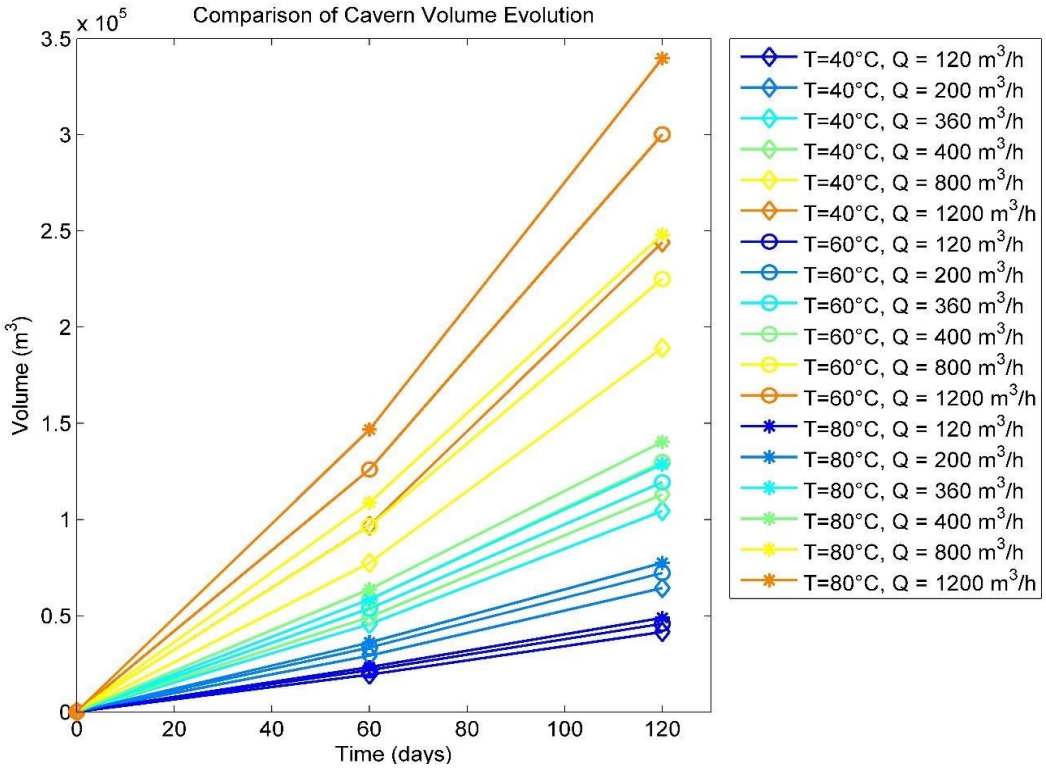

Source: The Autor (2022).

Figures 34 and 35 represent a comparison in the final time (120 days) between scenarios D and R from the highest temperature (80°C) and highest injection rate (1200 m³/h). It is observed that the largest radius and also the largest volume are reached for the R scenario. In addition, in terms of shape, the final contour for the D scenario has a more regular shape, while for the R scenario, there is a funneling and then further growth.

Figure 34 – Comparison of Final Contours: Direct x Reverse

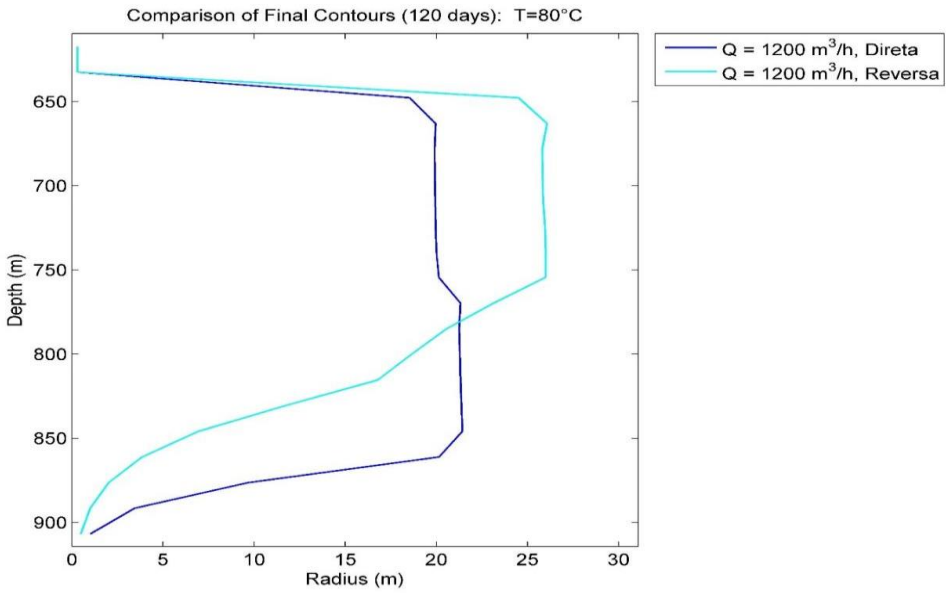

Source: The Autor (2022).

Figure 35 – Comparison of Cave Volume Evolution: Direct x Reverse

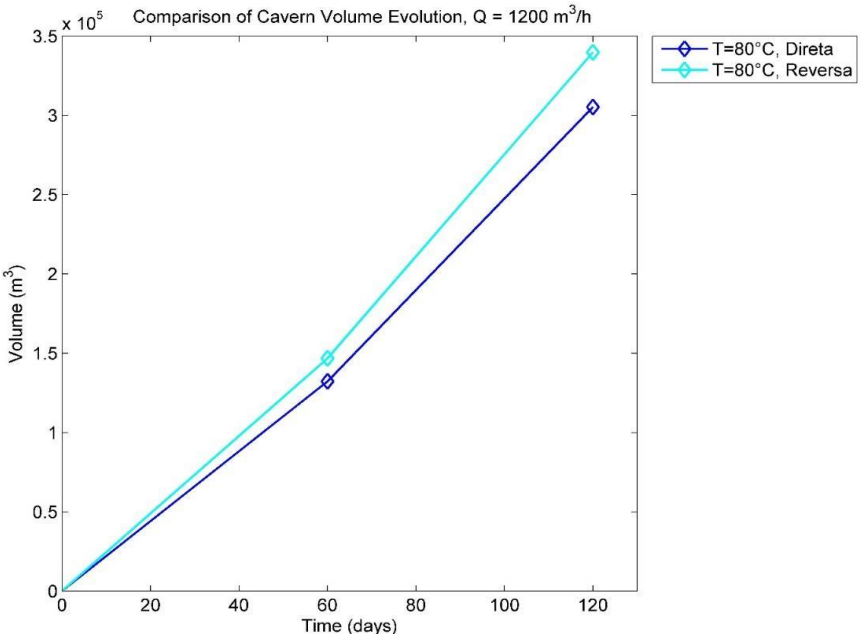

Source: The Autor (2022).

6.2 RESULTS WITH PCA

For each of the scenarios studied, statistical analysis of the data was performed considering the principal components technique. The main results are presented below.

- **SCENARIO D**

For scenario D, Table 9 presents the respective eigenvalues and the percentages of variance explained by each one. In the study with 11 parameters of simulations for the opening of a cavern in salt rock by dissolution, it was found that only two principal components are sufficient to explain 97% of the total variance of the parameters, in which PC1 was responsible for 79,04% and the second, PC2, for 18,04% of the data variations.

Comparatively, in a study with 7 criminality characteristics of some cities in the United States, it was found that with only two components it was possible to explain 68.13% of the total variance of the characteristics (HONGYU, 2015).

JOHNSON & WICHERN (1998), emphasize that it is sufficient for the retained components to represent at least 80% of the total variability of the data. Despite the first component (PC1) representing 79.04% of the total variability of the data, according to Table 10, the injection temperature parameter data has significant weight for the second component (PC2), around 70%, which justifies that this component is also considered in the study of the data set.

Table 9 – Principal Components (PCs), eigenvalues (λ) and percentage of variance explained by the components

PC	Eigenvalue	% Variance
1	8.69491	79.045
2	1.98493	18.045
3	0.26294	2.3904

Source: The Autor (2022).

To understand the importance of each variable in the construction of the two components, two important relationships were shown in Table 10, the weighting

coefficient, that is, the weight of each variable in the component under analysis and its correlation coefficients with the first two components main. As previously mentioned, the injection temperature variable has a significant weight in terms of the second component (PC2), not influence on the first component (PC1), the salt dissolution factor has similar comportment to injection temperature, it's happened because this coefficient depends directly on the temperature according to Eq. (3,7), the other variables have almost similar weight for PC1, even in PC2, radius and volume also have a small weight for the second component. As for the correlation, the injection temperature and DF are directly correlated to the y axis, while the other variables are directly correlated to the x-axis.

Table 10 – Weighting coefficients of the characteristics and their correlation coefficients with the first two principal components

	Weighting Coefficient		**Correlation**	
Principal Component	PC 1	PC 2	PC1	PC2
Injection Temperature	0.026337	0.6988	0.07766	0.98453
Injection Rate	0.33591	-0.053025	0.9905	-0.074706
Radius	0.32133	0.094616	0.94752	0.1333
Volume	0.32742	0.096823	0.96546	0.13641
Pump Power	0.33103	-0.052234	0.97611	-0.073591
Cumulative Energy	0.33056	-0.054977	0.97473	-0.077455
Tubing Loss	0.3369	-0.056195	0.99341	-0.079172
Produced Brine	0.33582	-0.052931	0.99022	-0.074573
Pump Pressure	0.33701	-0.048399	0.99374	-0.068188
Injection Pressure	0.33588	-0.06052	0.99042	-0.085265
Salt Dissolution Factor	0.067061	0.68762	0.19774	0.96877

Source: The Autor (2022).

From a set of 11 parameters, the dimensionality was reduced to just two principal components, whose equations are given by eq. (18) and (19):

$$PC1 = 0.03X_1 + 0.34X_2 + 0.32X_3 + 0.33X_4 + 0.33X_5 + 0.33X_6 + 0.34X_7 + 0.34X_8 + 0.34X_9 + 0.34X_{10} + 0.07X_{11} \quad (18)$$

$$PC2 = 0.70X_1 - 0.05X_2 + 0.10X_3 + 0.10X_4 - 0.05X_5 - 0.06X_6 - 0.05X_7 - 0.05X_8 - 0.06X_9 + 0.69X_{11} \quad (19)$$

X_1: Injection Temperature; X_2: Injection Rate; X_3: Radius; X_4: Volume; X_5: Pump Power; X_6: Cumulative Energy; X_7: Tubing Loss; X_8: Produced Brine; X_9: Pump Pressure; $X1_0$: Injection Pressure; $X1_1$: Salt Dissolution Factor.

Through Figure 6, a PC1 x PC2 biplot, it is possible to observe a high correlation between the variables injection rate, pump power, cumulative energy, tubing loss, produced brine, injection pressure, and pump pressure, as they are almost overlapping each other, the radius and volume variables also show a high correlation with each other. From the position in the biplot, it is noted that the injection temperature variable is isolated, next to DF, quite close to the y-axis, although they are in the same quadrant of the radius and volume, the latter doesn't seem to have a great contribution in terms of PC2.

Still in figure 36, it was also observed that in terms of PC1, x axis, the simulations further to the right were the ones that most contributed to the opening of the salt cavern, and in terms of PC2, y axis, the simulations further up the axis were those who contributed the most. As these components are orthogonal to each other, the variation explained in PC1 is independent of the variation explained in PC2 and so on if more components were considered.

Figure 36 – PC1 x PC2 Biplot

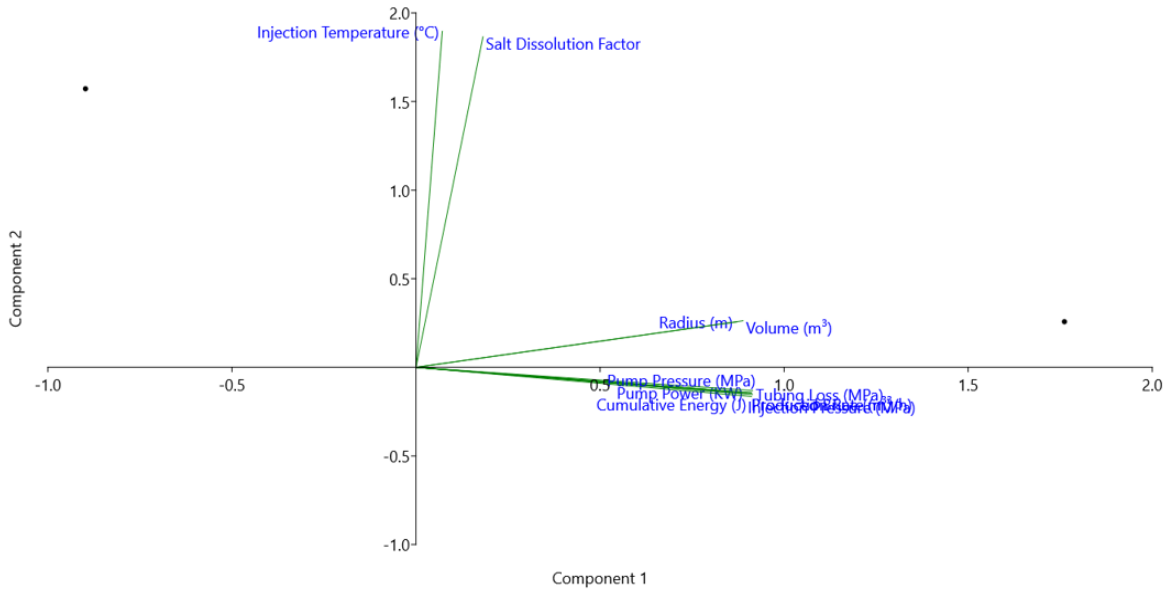

Source: The Autor (2022).

- **SCENARIO R**

For scenario R, the results with the PCA technique were quite similar to those of scenario D, in table 11, below, it is observed that 78,97% of the data are in terms of the first component (PC1), 17,88% in terms of the second (PC2), adding up to a total of almost 97% of variance in terms of the first two components.

Similarly to what happens in scenario D, the temperature in scenario R also has a significant weight in terms of the second component, around 70%, as shown in table 12. Therefore, both components (PC1 and PC2) must be considered in the data analysis of this population.

Table 11 – Principal Components (PCs), eigenvalues (λ) and percentage of variance explained by the components

PC	Eigenvalue	% Variance
1	8.68696	78.972
2	1.96689	17.881
3	0.273911	2.4901

Source: The Autor (2022).

Table 12 also shows that for PC1, the radius variable, which in scenario D had a weight and a correlation almost in the same proportion as the other variables, except injection temperature and DF, in this scenario appears to have a slightly smaller participation. On the other hand, it increased its share in terms of the second component.

Table 12 – Weighting coefficients of the characteristics and their correlation coefficients with the first two principal components

	Weighting Coefficient		Correlation	
Principal Component	PC 1	PC 2	PC1	PC2
Injection Temperature	0.02688	0.69881	0.079224	0.98005
Injection Rate	0.33594	-0.054279	0.99012	-0.076124
Radius	0.31809	0.11815	0.93754	0.1657
Volume	0.32906	0.083291	0.96987	0.11681
Pump Power	0.33053	-0.059279	0.97419	-0.083137
Cumulative Energy	0.33056	-0.060614	0.97427	-0.085009
Tubing Loss	0.33682	-0.060065	0.99274	-0.084239
Produced Brine	0.33583	-0.054172	0.98983	-0.075975
Pump Pressure	0.33688	-0.054571	0.99291	-0.076534
Injection Pressure	0.33604	-0.062936	0.99044	-0.088265
Salt Dissolution Factor	0.076151	0.68349	0.22444	0.95856

Source: The Autor (2022).

Equations 20 and 21 below are the equations for the first two components in scenario R:

$$PC1 = 0.03X_1 + 0.34X_2 + 0.32X_3 + 0.33X_4 + 0.33X_5 + 0.33X_6 + 0.34X_7 + 0.34X_8 + 0.34X_9 + 0.34X_{10} + 0.08X_{11} \quad (20)$$

$$PC2 = 0.70X_1 - 0.05X_2 + 0.12X_3 + 0.08X_4 - 0.06X_5 - 0.06X_6 - 0.05X_7 - 0.05X_8 - 0.06X_9 + 0.68X_{11} \quad (21)$$

By the PC1 x PC2 Biplot, Figure 37, it is possible to observe that in terms of PC1, the variables injection rate, pump power, cumulative energy, tubing loss, produced brine, injection pressure, and pump pressure maintain a high correlation between them, also in the R scenario. The radius and volume variables decreased the correlation between them, compared to the D scenario. For PC2, the temperature and DF remained very close to the y axis, with the radius variable closer to the y axis as well.

As for the simulations, in terms of PC1, the increase in production rate continued to be the factor that most contributed to the opening of the cave, while for PC2, the temperature exerted this influence.

Figure 37 – PC1 x PC2 Biplot

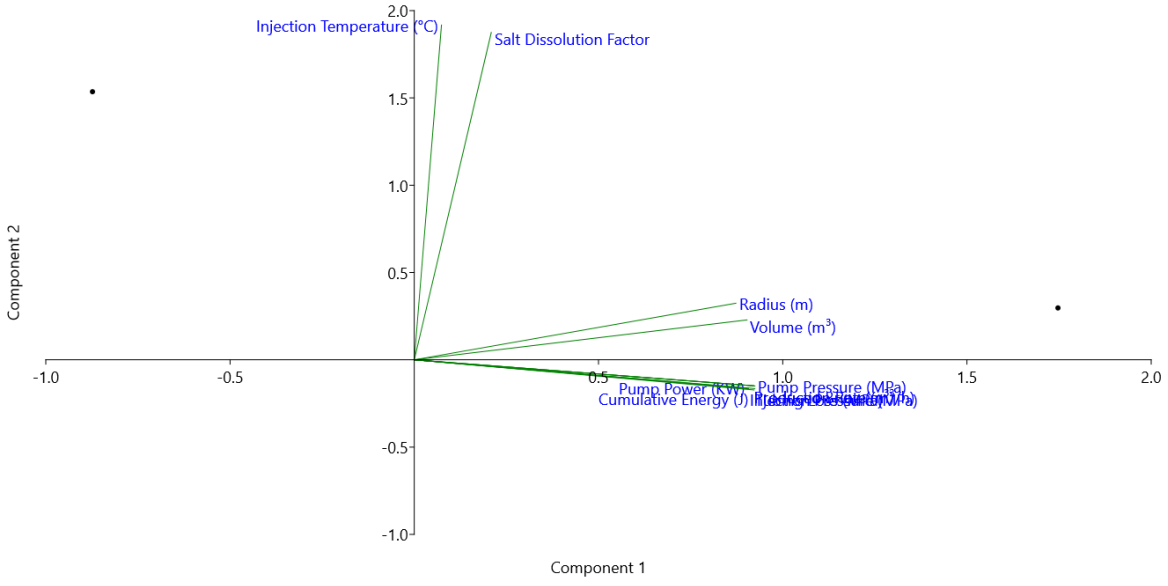

Source: The Autor (2022).

6.3 RELATION DF x INJECTION TEMPERATURE x INJECTION RATE

Another important relation it's DF x Injection Temperature x Injection Rate. Considering the temperatures of 40, 60, and 80 °C for the respective injection rates and salt dissolution factors, it is possible to trace a graphic analyzing each scenario.

Figures 38 and 39 suggest low temperatures, 40°C, DF doesn't change with an increase in injection rates, it's possible to see any changes from the injection rate of 400 m³/h and injection temperature of 80°C. Similar behavior was observed in both scenarios.

Table 13 – Data of DF, Injection Temperature, and Injection Rate to Scenario D

40°C		60°C		80°C	
Q	**DF**	**Q**	**DF**	**Q**	**DF**
120	1.259894	120	1.58798	120	1.670901
200	1.26017	200	1.590177	200	1.676977
360	1.260719	360	1.591269	360	1.68872
400	1.260993	400	1.592356	400	1.694402
800	1.263961	800	1.604033	800	1.750297
1200	1.268407	1200	1.622144	1200	1.824287

Source: The Autor (2022).

Table 14 – Data of DF, Injection Temperature and Injection Rate to Scenario R

40°C		60°C		80°C	
Q	**DF**	**Q**	**DF**	**Q**	**DF**
120	1.258226	120	1.581274	120	1.630975
200	1.258506	200	1.582404	200	1.638101
360	1.258785	360	1.584649	360	1.651749
400	1.259063	400	1.585764	400	1.658297
800	1.262351	800	1.598788	800	1.726229
1200	1.267375	1200	1.618217	1200	1.809206

Source: The Autor (2022).

Figure 38 - DF x Injection Temperature x Injection Rate to Scenario D

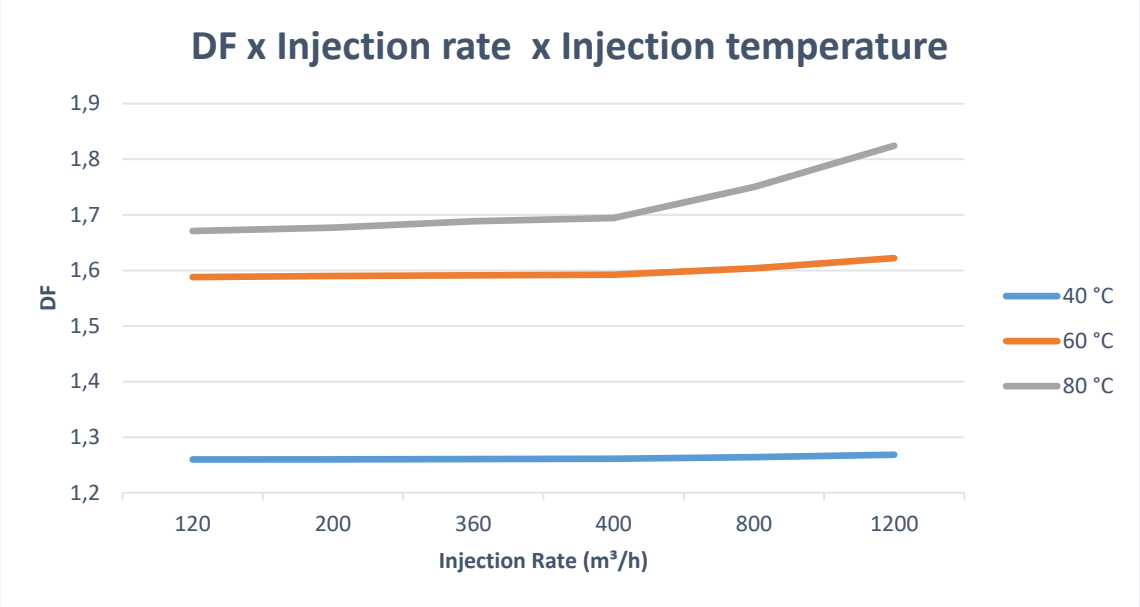

Source: The Autor (2022).

Figure 39 – DF x Injection Temperature x Injection Rate to Scenario R

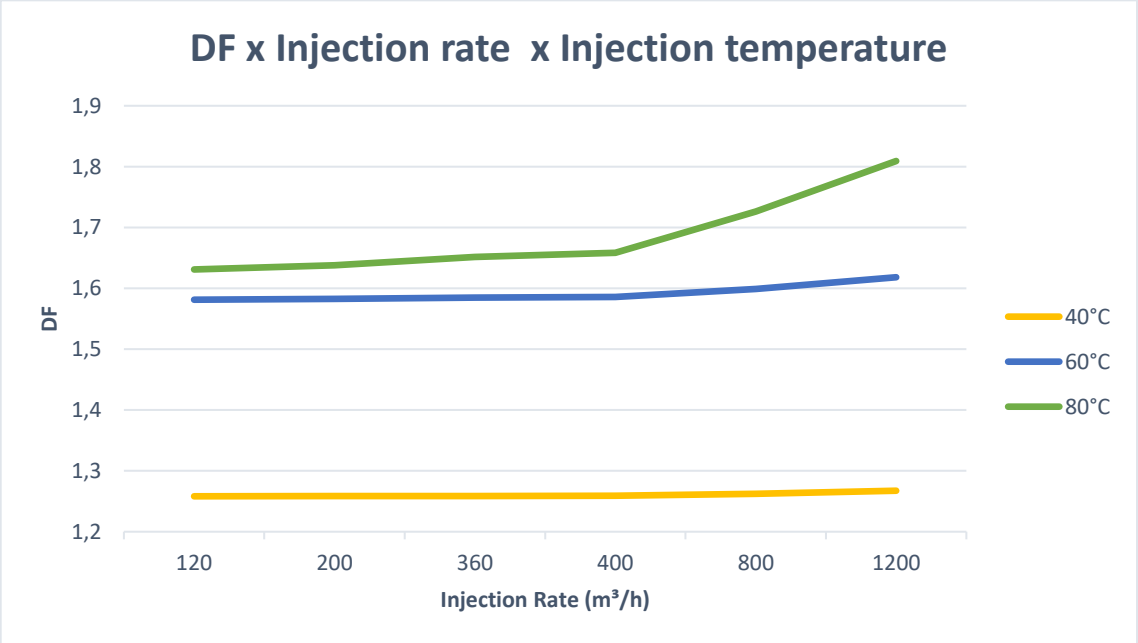

Source: The Autor (2022).

7 CONCLUSIONS

Taking into account the results obtained, the principal component analysis technique proved to be effective and allowed the removal of nine variables that were redundant because they were correlated with others of greater importance, that is, the 11 parameters of the numerical simulations in SalGas reduced its dimensionality to two principal components, the brine injection rate provided the most information for the x-axis and the injection temperature the largest for the y-axis, in this way, the modeling process for new scenarios can be streamlined and simplified, preserving most of the original data. Added together, the first two components represented about 97% of the total variability of the original data.

As for the influence on the salt cavity opening process, in terms of PC1, the brine injection rate was the variable that most contributed to the process, being followed in the same proportion by the other variables, exception for the injection temperature and DF. These have a significant weight in terms of PC2. For the analysis of principal components, both scenarios presented almost similar results, as for the SALGAS simulations, in the proposed time of 120 days, the final geometry of the cave for the Scenario D resembled the appearance of a pear while for the Scenario R of a cone, the contour and the final volume of the cave were higher for the Scenario R, this does not imply that one scenario is more favorable than the other, since each one has its advantages and limitations.

With the numerical simulations, it was also possible to conclude that the largest radius and the largest volume were found for the simulation of a higher production rate, 1200m³/h, and higher temperature, 80°C, that is, the higher the brine injection rate, the greater the radius and volume of the cave. Similar behavior is verified in relation the influence of the injection temperature, the higher the temperature, the greater the volume and radius of the cavern, although it influences to a lesser extent. Also, when analyzing the relation of DF with injection temperature and injection rate, it’s possible to see that the variable temperature influences in the behavior of cavern for high temperatures and injection rates.

8 SUGGESTIONS AND FUTURE WORK

Despite the success with the simulations and the use of the principal component analysis technique, it is important to emphasize that for high temperatures, pressures and production rates it is necessary to carry out an experimental validation to obtain more realistic parameters such as the rate of dissolution of the rock. In this sense, carrying out experiments to validate such conclusions is a bet to improve this work in the future. Another important point is to consider in future studies a larger population of data, it would be interesting to apply both the PCA technique with more characteristics and number of observations, as well as other data analysis techniques and probabilistic models.

REFERENCES

ALKAN, H., MULLER, W., MINKLEY, W., GEBIRGSMECGANIK, I., & JOBMANN, M. (2010). A Benchmarking of the Numerical Approaches for the Stress-Dilatancy-Permeability Relationship in EDZ of Rock Salt. **Solution Mining Research Institute**, (October), pp. 1–14, 2010.

ALONSO-GUTIERREZ, J. et al. Principal component analysis of proteomics (PCAP) as a tool to direct metabolic engineering. **Metabolic Engineering**, v. 28, p. 123 – 133, 2015.

ATG Manuel pour le transport et la distribution du gaz. Titre XIII - Stockages souterrains de gaz. **Association Technique de l'Industrie du Gaz en France**, 1986.

BROUARD. SMRI Technical Class: Solution Mining and Hydrocarbon Storage Toolbox. **Solution Mining Research Institute**, 2008.

BROUARD, B., ZAKHAROV, V., & CONSULTING, B. Introducing LOCAS 3D Application to the Geomechanical Modeling of an Oil-Storage Facility, **Solution Mining Research Institute (SMRI)**, pp. 1–18, 2018.

COSTA, P.V.M. **Potencial de Estocagem Subterrânea de Gás Natural em Cavernas de Sal Abertas por Dissolução em Domo Salino Offshore no Brasil**.2018. 302f. Tese (Doutorado em Planejamento Energético) - Universidade Federal do Rio de Janeiro, Rio de Janeiro, 2018.

DE MELO, P. R. C.; DE CARVALHO, R. S.; & PINTO, D. C. Rochas e Minerais Industriais. **CETEM**, p. 1–24, 2008.

DONADEI, S.; & SCHNEIDER, G.,-S. Compressed Air Energy Storage in Underground Formations. **Storing Energy**, 113-133, 2016.

DONAT, G. F. Solutions Found to some Problems connected the Construction by Dissolution with of Natural Gas Storage Cavities in Salt. American Instite of Mining, pp. 1–11, 1972.

DURIE, R. W.; & JESSEN, F. W. Mechanism of the Dissolution of Salt in the Formation of Underground Salt Cavities. **Society of Petroleum Engineers Journal**, v. 4, n. 2, p. 183–190, 1964.

eCORP International, LLC. **Types of Storage**. Available in:

< http://www.ecorpintl.com/midstream/storage/types/>. Access in: 09,14,2021.

EYERMAN, T. SALGAS and SalGas for Windows User ' s Manual, pp. 1–53, 2008.

FAIRCHILD, I. J.; KILLAWEE, J. A.; HUBBARD, B.; & DREYBRODT,W. Interactions of calcareous suspended sediment with glacial meltwater: a file test of dissolution behaviour. **Chemical Geology**, v. 155, n. 3-4, p. 243–263, 1999.

FERREIRA, D.F. **Estatística Multivariada**.Lavras: UFLA, 2011.

FIRME, P. A. L. P.; ROEHL, D.; ROMANE, C. Salt caverns history and geomechanics towards future natural gas strategic storage in Brazil. **Journal of Natural Gas Science and Engineering**, 2019.

GE, X.; LI, Y.; CHEN, X.; SHI, X.; MA, H.; YIN, H.; ZHANG, N. and YANG, C. Dynamics of a Partially Confined, Vertical Upward-Fluid-Conveying, Slender Cantilever Pipe with Reverse External Flow. **Applied Science**, 2019.

HABIBI, R. An investigation into design concepts, design methods and stability criteria of salt caverns. **Oil & Gas Science and Technology** - Revue d'IFP Energies nouvelles, Institut Français du Pétrole, 74, p.14, 2019.

HAIR, J. F.; BLACK, W. C.; BABIN, B. J.; ANDERSON, R. E.; TATHAM R. L. **Análise multivariada de dados.** Brasil, Bookman, 2009.

HAMMER, O.; HARPER, D. & RYAN, P. PAST: PALEONTOLOGICAL STATISTICS SOFTWARE PACKAGE FOR EDUCATION AND DATA ANALYSIS. **Palaeontological Association**. June, 2021.

HAMZA, A.; HUSSEIN, I. A.; AL-MARRI, M. J.; MAHMOUD, M.; SHAWABKEH, R.; APARICIO, S. CO2 enhanced gas recovery and sequestration in depleted gas reservoirs: A review. **Journal of Petroleum Science and Engineering**, v. 196, pp. 1 – 24, 2021.

HONGYU, K.; SANDANIELO, V. L. M.; JUNIOR, G. J. Principal Component Analysis: theory, interpretations and applications. **E&S - Engineering and Science**, v.1, n. 5, pp. 83–90, 2015.

HOVORKA, S. D. Understanding the Processes of Salt Dissolution and Subsidence. **Solution Mining Research Institute (SMRI),** pp. 1–8, 2000.

HUANG, X., & XIONG, J. (2011). Numerical simulation of gas leakage in bedded salt rock storage cavern. **Procedia Engineering**, n.12, pp. 254–259. https://doi.org/10.1016/j.proeng.2011.05.040

JEREMIC, M.L. Rock mechanics in salt mining, 1st ed. A. A. Balkema Publishers, Rotterdam, 1994.

JIANG, D.; LI, Z.; LIU, W.; BAN, F.; CHEN, J.; WANG, Y.; FAN, J. Construction simulating and controlling of the two-well-vertical(TWV) salt caverns with gas blanket. **Journal of Natural Gas Science and Engineering**, v. 96, 2021.

JIANG, D. Y.; YI, L.; CHEN, J.; REN, S.; QIU, H. F.; & LI, Y. P. Laboratory similarity test relevant to salt cavern construction in interlayer-containing moulded saliferous aggregates specimen. **Current Science**, v. 111(1), p. 157–167, 2016.

JINPING, Y.; GUANJIE, Y.; & GENSHENG, L. Research and application of quich-speed solution mining technique and tool. **Geotechnical Engineering, C**, p. 1–8, 2008.

JOHNSON, R.A.; WICHERN, D.W. Applied multivariate statistical analysis.Madison: Prentice Hall International, 816p. , 1998.

KAZARYAN, V., SALOKHIN, V., & SHECHERBAK, S. Solution Mining of Underground Storage in Rock of Limited Thickness : Experience and Computer Simulation. **Solution Mining Research Institute (SMRI),** pp. 1–14, 2007.

KOHLER, M. R. **Redes Neurais Aplicadas à Construção de Aproximadores para Simulação Integrada entre Reservatório e Sistema de Produção**. 2013. 96 f. Dissertação (Mestrado em Engenharia Elétrica) – Pontifícia Universidade Católica do Rio de Janeiro, Rio de Janeiro, 2013.

KUNSTMAN, A. S., & URBANCZYK, K. M. A computer model for designing salt cavern leaching process developed at Chemkop. **Solution Mining Research Institute (SMRI)**, pp. 1–17, 1990.

LI, J., SHI, X., WANG, T., YANG, C., LI, Y., MA, H., … SHI, H. A prediction model of the accumulation shape of insoluble sediments during the leaching of salt cavern for gas storage. **Journal of Natural Gas Science and Engineering**, v. 33, pp. 792–802, 2016.

LI, J., SHI, X., YANG, C., LI, Y., WANG, T., & MA, H. Mathematical model of salt cavern leaching for gas storage in high-insoluble salt formations. **Scientific Reports**, v. 8(1), pp. 1–12, 2018.

LIU, X.; YANG, X.; WANG, J.; LI, D.; LI, P.; & YANG, Z. A dynamic dissolution model of rock salt under gravity for different flow rates. **Arabian Journal of Geosciences**, v. 9, n. 3, p. 1–8, 2016.

LIU, W.; LI, Y. P.; & YANG , C. H. Permeability characteristics of mudstone cap rock and interlayers in bedded salt formations and tightness assessment for underground gas storage caverns. **Eng. Geol.**, v. 193, p. 212-223, 2015.

LIU,W.; ZHANG, Z.; CHEN ,J.; & JIANG, D. Feasibility evalution of large-scale underground hydrogen storage in bedded salt rocks of China: A case study in Jiangsu province. **Energy**, v. 198, p. 1–16, 2020.

MOKHATAB, S.; POE, W., A.; & MAK, J.,Y. Handbook of Natural Gas Transmission and Processing. 4. ed., 2019.

NAZARY MOGHADAM, S.; MIRZABOZORG, H.; NOORZAD, A. Modeling time dependent behavior of gas caverns in rock salt considering creep, dilatancy and failure. **Tunneling and Underground Space Technology**, v. 33, p. 171–185, 2013.

NAZARY MOGHADAM, S.; NAZOKKAR, K; CHALATURNYK, R. K.; & MIRZABOZORG, H. Parametric assessment of salt cavern performance using a creep model describing dilatancy and failure. **International Journal of Rock Mechanics and Mining Sciences**, v. 79, p. 250–267, 2015.

PATTERSON J.B.; MORRIS E. Measurement of Absolute Water Density, 1°C to 40°C. **Metrologia**, 1994.

QUERIO, C. W.; STEINER, M. E.; & DURNELL, W. E. Expansion of Solution Cavern Storage Technology. **SPE**, p. 1–12, 1981.

REGAZZI, A.J. Análise multivariada, notas de aula INF 766, Departamento de Informática da Universidade Federal de Viçosa, v.2, 2000.

SABERIAN, A. Numerical Simulation of Development of Solution-Mined Salt Cavities. **Solution Mining Research Institute**, 1974.

SABERIAN, A. SMRI Research Project Report nº 83-0002: A dissolution/ temperature relation for vertical salt surfaces dissolved in saline solutions. **Solution Mining Research Institute**, 1983.

SMIRNOV, V.; KAZARYAN, V.; POZDNYAKAV, A.; IGOSHIN, A.; & MALJUKOV, V. Method for Experimental Determination of Rock Salt Dissolution Rate Coefficient used in Podzemgasprom. **Ltd. Solution Mining Research Institute**, p. 1–12, 2002.

TIAN, Z., Wang, T., & Zhang, G. Key technologies research of natural gas storage construction in salt rock formation. **Rock Stress and Earthquakes**, p. 469–474, 2010.

U. S. Department of Energy. **SPR Storage Sites**, 2020. Available in: <https://www.energy.gov/fe/services/petroleum-reserves/strategic-petroleum-reserve/spr-storage-sites>. Access in: 09,14,2021.

VARELLA, C. A. A. Análise Multivariada Aplicada as Ciências Agrárias: Análise de Componentes Principais. Pós-Graduação em Agronomia – Universidade Federal Rural do Rio de Janeiro, 2008.

WAN, J.; PENG, T.; SHEN, R.; JURADO, M.J. Numerical Model and Program Development of TWH Salt Cavern Construction for UGS. **Journal of Petroleum Science and Engineering**, pp. 1–27, 2019.

WAN, J.; PENG, T.; YUAN, G.; BAN, F.; JURADO, M.J.; XIA, Y. Influence of tubing/oil-blanket lifting on construction and geometries of two-well-horizontal salt caverns. **Tunnelling and Underground Space Technology**, v.108, pp. 1–11 2021.

WANG, T.; DING, S.; WANG, H.; YANG, C.; SHI, X.; MA, H.; & DAEMEN, J. J. K. Mathematic modelling of the debrining for a salt cavern gas storage. **Journal of Natural Gas Science and Engineering**, v. 50, pp. 205–214, 2018.

WARREN, J, K. **Evaporites: Sediments, Resources and Hydrocarbons**. Berlin: Springer, 2006, pp. 1-1036.

WEISBROD, N.; ALON-MORDISH, C.; KONEN, E.; YECHIELI, Y. Dynamic dissolution of halite rock during flow of diluted saline solutions. **Geophysical Research Letters**, p. 1–7, 2012.

YANG, C.; DAEMEN, J. J. K.; & YIN, J. H. Experimental investigation of creep behavior of salt rock. **Int. J. Rock. Mech. Min. Sci.**, v. 36, p. 233-242, 1999.

YANG, XIN; LIU, X. Numerical simulation of rock salt dissolution in dynamic water. **Environ Earth Sci**, pp. 1–10, 2017.

YANG, X.; LIU, X.; ZANG, W.; LIN, Z.; & WANG, Q. A Study of Analytical Solution for the Special Dissolution Rate Model of Rock Salt. **Hindawi**, p. 1–9, 2017.

YIN, H.; YANG, C., MA, H., SHI, X.; ZHANG, N.; GE, X.; … HAN, Y. Stability evaluation of underground gas storage salt caverns with micro-leakage interlayer in bedded rock salt of Jintan, China. **Acta Geotechnica**, p. 1–15, 2020.

APPENDIX A – INPUT DATA FOR SALGAS

The sequence of figures describes the structure of SalGas input data for hypothetical scenarios.

INPUT DATA: *.sgi

➢ FIRST LINE – 2 INPUTS

- 1.1 **MSYS**: An integer to indicate the unit of measurements, " 0" for American/Imperial units, " 1" for metric;
- 1.2 **TITLE**: An alphanumeric field for the title of the run or something that is pertinent to inform for you better identification.

```
0   Cenário D 120m³/h 40C
0 20 2 60 0 0 0 3 3000.000000 2500.000000
1000.000000 2000.000000 2.160000 10.750000 7.000000 2100.000000 1.300000 0.000000
60.000000 510.740000 1.000000 1.196300 1.023930 1.259894 0.030000
1 2 2 1 15.000000 0.000130 0.900000
100 8
2800 6
200 6
2400 9.9 7.0
100 9.9 7.8
100 8
```

.

INPUT DATA: *.sgi

➢ SECOND LINE – 10 INPUTS

- 2.1 **ICODE**: An indicator for the initial direction of mining, " 0" for direct and " 1" for reverse. For Scenario D, use " 0" and for Scenario R, use "'1";
- 2.2 **N**: Number of cells (elements) for modeling the cavern interval, 200 maximum ;
- 2.3 **M**: Number of time intervals with changes in parameters of cave, 50 maximum .

```
0   Cenário D 120m³/h 40C
0 20 2 60 0 0 0 3 3000.000000 2500.000000
1000.000000 2000.000000 2.160000 10.750000 7.000000 2100.000000 1.300000 0.000000
60.000000 510.740000 1.000000 1.196300 1.023930 1.259894 0.030000
1 2 2 1 15.000000 0.000130 0.900000
100 8
2800 6
200 6
2400 9.9 7.0
100 9.9 7.8
100 8
```

.

INPUT DATA: *.sgi

➢ SECOND LINE – 10 INPUTS

- 2.4 **IDT**: Time interval in days at which the production (and hydraulic and gas pad as requested) data is to be printed;
- 2.5 **IPAD**: Indictor if blanket is present, “0” if there is a blanket, “1” if there is no blanket.

```
0   Cenário D 120m³/h 40C
0 20 2 60 0 0 0 3 3000.000000 2500.000000
1000.000000 2000.000000 2.160000 10.750000 7.000000 2100.000000 1.300000 0.000000
60.000000 510.740000 1.000000 1.196300 1.023930 1.259894 0.030000
1 2 2 1 15.000000 0.000130 0.900000
100 8
2800 6
200 6
2400 9.9 7.0
100 9.9 7.8
100 8
```

.

INPUT DATA: *.sgi

➢ SECOND LINE – 10 INPUTS

- 2.6 **ISOR**: Indicates if there are changes in mining direction at any time during the model run. “0” if there are no changes, “1” if there are changes;
- 2.7 **ICON**: Type of roof pad, “0” if the pad is incompressible (liquid), “1” if compressible (gas).

```
0   Cenário D 120m³/h 40C
0 20 2 60 0 0 0 3 3000.000000 2500.000000
1000.000000 2000.000000 2.160000 10.750000 7.000000 2100.000000 1.300000 0.000000
60.000000 510.740000 1.000000 1.196300 1.023930 1.259894 0.030000
1 2 2 1 15.000000 0.000130 0.900000
100 8
2800 6
200 6
2400 9.9 7.0
100 9.9 7.8
100 8
```

.

INPUT DATA: *.sgi

➢ SECOND LINE – 10 INPUTS

- 2.8 **ISHORT**: Simulation selector, "0" if mining only, "1" if mining, hydraulics and gas pad calculations, "2" for mining and gas pad calculations, "3" for mining and hydraulics only. As ISHORT= 3, the hydraulic model was activated, being necessary to insert the extra data in the 10th conditional input module.

```
0   Cenário D 120m³/h 40C
0 20 2 60 0 0 0 3 3000.000000 2500.000000
1000.000000 2000.000000 2.160000 10.750000 7.000000 2100.000000 1.300000 0.000000
60.000000 510.740000 1.000000 1.196300 1.023930 1.259894 0.030000
1 2 2 1 15.000000 0.000130 0.900000
100 8
2800 6
200 6
2400 9.9 7.0
100 9.9 7.8
100 8
```

.

INPUT DATA: *.sgi

➢ SECOND LINE – 10 INPUTS

- 2.9 **DEPINJ**: Depth (in feet or meters) to the initial injection point;
- 2.10 **DEPPRD**: Depth (in feet or meters) to the initial production point;

The values from tab. (4) are considered for each of the scenarios.

```
0   Cenário D 120m³/h 40C
0 20 2 60 0 0 0 3 3000.000000 2500.000000
1000.000000 2000.000000 2.160000 10.750000 7.000000 2100.000000 1.300000 0.000000
60.000000 510.740000 1.000000 1.196300 1.023930 1.259894 0.030000
1 2 2 1 15.000000 0.000130 0.900000
100 8
2800 6
200 6
2400 9.9 7.0
100 9.9 7.8
100 8
```

.

INPUT DATA: *.sgi

➢ THIRD LINE – 8 INPUTS

- 3.1 **H**: Height of the salt section (in feet or meters);
- 3.2 **DEPT**: Depth (in feet or meters) to top of modeled interval;
- 3.3 **DENSAL**: Specific Gravity of salt (2.16 default). Changing this value will impact the rate at which salt is dissolve.

```
0  Cenário D 120m³/h 40C
0 20 2 60 0 0 0 3 3000.000000 2500.000000
1000.000000 2000.000000 2.160000 10.750000 7.000000 2100.000000 1.300000 0.000000
60.000000 510.740000 1.000000 1.196300 1.023930 1.259894 0.030000
1 2 2 1 15.000000 0.000130 0.900000
100 8
2800 6
200 6
2400 9.9 7.0
100 9.9 7.8
100 8
```

INPUT DATA: *.sgi

➢ THIRD LINE – 8 INPUTS

- 3.4 **DP**: Outside diameter (in inches or millimeters) of outer, shallower tubing string;
- 3.5 **DPT**: Outside diameter (in inches or millimeters) of inner, deeper tubing string;
- 3.6 **DEPPAD**: Depth to the roof pad (in meters or feet) if the roof pad level is not moved during modeled time period.

```
0  Cenário D 120m³/h 40C
0 20 2 60 0 0 0 3 3000.000000 2500.000000
1000.000000 2000.000000 2.160000 10.750000 7.000000 2100.000000 1.300000 0.000000
60.000000 510.740000 1.000000 1.196300 1.023930 1.259894 0.030000
1 2 2 1 15.000000 0.000130 0.900000
100 8
2800 6
200 6
2400 9.9 7.0
100 9.9 7.8
100 8
```

INPUT DATA: *.sgi

➢ THIRD LINE – 8 INPUTS

- 3.7 **BULK**: Bulking factor of insolubles on floor of cavern, (default 1.3 if no value is entered);
- 3.8 **DPINS**: Depth (in meters or feet) from surface to the level of accumulated insolubles on the floor of the cavern. If there are no insolubles at the start of the run enter "0.0".

```
0  Cenário D 120m³/h 40C
0 20 2 60 0 0 0 3 3000.000000 2500.000000
1000.000000 2000.000000 2.160000 10.750000 7.000000 2100.000000 1.300000 0.000000
60.000000 510.740000 1.000000 1.196300 1.023930 1.259894 0.030000
1 2 2 1 15.000000 0.000130 0.900000
100 8
2800 6
200 6
2400 9.9 7.0
100 9.9 7.8
100 8
```

.

INPUT DATA: *.sgi

➢ FOURTH LINE – 7 INPUTS

- 4.1 **CONTPD**: Time interval (in days) for printout of Cavity data (shape, brine specific gravity) and times at which the mining direction (direct or reverse) may be changed;
- 4.2 **CONQUE**: Rate of brine production (in gallons per minute or cubic meters per hour) from cavern. For each Scenario, use the production rates in tables 5 and 6.

```
0  Cenário D 120m³/h 40C
0 20 2 60 0 0 0 3 3000.000000 2500.000000
1000.000000 2000.000000 2.160000 10.750000 7.000000 2100.000000 1.300000 0.000000
60.000000 510.740000 1.000000 1.196300 1.023930 1.259894 0.030000
1 2 2 1 15.000000 0.000130 0.900000
100 8
2800 6
200 6
2400 9.9 7.0
100 9.9 7.8
100 8
```

.

INPUT DATA: *.sgi

➢ FOURTH LINE – 7 INPUTS

- 4.3 **CONRAD**: Initial radius of cavern (feet or meters). This must be greater than the diameter of the outer tubing string;
- 4.4 **CONSGB**: Initial specific gravity of brine in cavern. For each Scenario, use the initial specific gravity of brine in tables 5 and 6.

```
0   Cenário D 120m³/h 40C
0 20 2 60 0 0 0 3 3000.000000 2500.000000
1000.000000 2000.000000 2.160000 10.750000 7.000000 2100.000000 1.300000 0.000000
60.000000 510.740000 1.000000 1.196300 1.023930 1.259894 0.030000
1 2 2 1 15.000000 0.000130 0.900000
100 8
2800 6
200 6
2400 9.9 7.0
100 9.9 7.8
100 8
```

.

INPUT DATA: *.sgi

➢ FOURTH LINE – 7 INPUTS

- 4.5 **CONISG**: Specific gravity of injection water. For each Scenario, use the specific gravity of injection water in tables 5 and 6;
- 4.6 **CONDIS**: Dissolution factor of salt. For each Scenario, use the dissolution factor in tables 5 e 6;
- 4.7 **VINSL**: Percentage of insolubles in salt entered as decimal.

```
0   Cenário D 120m³/h 40C
0 20 2 60 0 0 0 3 3000.000000 2500.000000
1000.000000 2000.000000 2.160000 10.750000 7.000000 2100.000000 1.300000 0.000000
60.000000 510.740000 1.000000 1.196300 1.023930 1.259894 0.030000
1 2 2 1 15.000000 0.000130 0.900000
100 8
2800 6
200 6
2400 9.9 7.0
100 9.9 7.8
100 8
```

.

INPUT DATA: *.sgi

➢ OPTIONAL HYDRAULICS MODEL INPUT

✓ This data is required when ISHORT (8th value on 2nd line) equals “1” or “3”.

➢ FIRST LINE – 7 INPUTS

- **I1**: Number of sections to be modeled in the surface brine line.

```
0   Cenário D 120m³/h 40C
0 20 2 60 0 0 0 3 3000.000000 2500.000000
1000.000000 2000.000000 2.160000 10.750000 7.000000 2100.000000 1.300000 0.000000
60.000000 510.740000 1.000000 1.196300 1.023930 1.259894 0.030000
1 2 2 1 15.000000 0.000130 0.900000
100 8
2800 6
200 6
2400 9.9 7.0
100 9.9 7.8
100 8
```

INPUT DATA: *.sgi

➢ FIRST LINE – 7 INPUTS

- **J1**: Number of sections to be modeled in cavern inner tubing string.
- **K1**:Number of sections to be modeled in cavern outer tubing string.
- **L1**: Number of sections to be modeled in surface water line.

```
0   Cenário D 120m³/h 40C
0 20 2 60 0 0 0 3 3000.000000 2500.000000
1000.000000 2000.000000 2.160000 10.750000 7.000000 2100.000000 1.300000 0.000000
60.000000 510.740000 1.000000 1.196300 1.023930 1.259894 0.030000
1 2 2 1 15.000000 0.000130 0.900000
100 8
2800 6
200 6
2400 9.9 7.0
100 9.9 7.8
100 8
```

INPUT DATA: *.sgi

➢ FIRST LINE – 7 INPUTS

- **PDEL**: Brine delivery pressure at the end of the surface brine line (psi or mPa);
- **ROUGH**: Surface roughness of pipe (in inches/inch or millimeters/millimeter);
- **EPUMP**: Efficiency of water pump. This value needs to be entered as a decimal for input file.

```
0  Cenário D 120m³/h 40C
0 20 2 60 0 0 0 3 3000.000000 2500.000000
1000.000000 2000.000000 2.160000 10.750000 7.000000 2100.000000 1.300000 0.000000
60.000000 510.740000 1.000000 1.196300 1.023930 1.259894 0.030000
1 2 2 1 15.000000 0.000130 0.900000
100 8
2800 6
200 6
2400 9.9 7.0
100 9.9 7.8
100 8
```

.

INPUT DATA: *.sgi

➢ SECOND LINE – 2 INPUTS

- 2.1: Surface brine line segment length (in feet or meters);
- 2.2: The inside diameter of the segment (in i nches or millimeters).

```
0  Cenário D 120m³/h 40C
0 20 2 60 0 0 0 3 3000.000000 2500.000000
1000.000000 2000.000000 2.160000 10.750000 7.000000 2100.000000 1.300000 0.000000
60.000000 510.740000 1.000000 1.196300 1.023930 1.259894 0.030000
1 2 2 1 15.000000 0.000130 0.900000
100 8
2800 6
200 6
2400 9.9 7.0
100 9.9 7.8
100 8
```

.

INPUT DATA: *.sgi

➢ THIRD AND FOURTH LINE – 2 INPUTS (J1=2)

- 3.1 e 4.1:Inner tubing segment length (in feet or meters);
- 3.2 e 4.1: Inside diameter of inner tubing (in inches or millimeters).

```
0  Cenário D 120m³/h 40C
0 20 2 60 0 0 0 3 3000.000000 2500.000000
1000.000000 2000.000000 2.160000 10.750000 7.000000 2100.000000 1.300000 0.000000
60.000000 510.740000 1.000000 1.196300 1.023930 1.259894 0.030000
1 2 2 1 15.000000 0.000130 0.900000
100 8
2800 6
200 6
2400 9.9 7.0
100 9.9 7.8
100 8
```

INPUT DATA: *.sgi

➢ FIFTH AND SIXTH LINE – 3 INPUTS (K1 =2)

- 5.1 e 6.1: Outer tubing segment length (in feet or meters);
- 5.2 e 6.2: Inside diameter of inner tubing (in inches or millimeters);
- 5.3 e 6.3: Outside diameter of outer tubing (in inches or millimeters).

```
0  Cenário D 120m³/h 40C
0 20 2 60 0 0 0 3 3000.000000 2500.000000
1000.000000 2000.000000 2.160000 10.750000 7.000000 2100.000000 1.300000 0.000000
60.000000 510.740000 1.000000 1.196300 1.023930 1.259894 0.030000
1 2 2 1 15.000000 0.000130 0.900000
100 8
2800 6
200 6
2400 9.9 7.0
100 9.9 7.8
100 8
```

INPUT DATA: *.sgi

➢ SEVENTH LINE – 2 INPUTS

- 7.1: Surface water line segment length (in feet or meters);
- 7.2: The inside diameter of the segment (in inches or millimeters).

```
0  Cenário D 120m³/h 40C
0 20 2 60 0 0 0 3 3000.000000 2500.000000
1000.000000 2000.000000 2.160000 10.750000 7.000000 2100.000000 1.300000 0.000000
60.000000 510.740000 1.000000 1.196300 1.023930 1.259894 0.030000
1 2 2 1 15.000000 0.000130 0.900000
100 8
2800 6
200 6
2400 9.9 7.0
100 9.9 7.8
100 8
```

.